Eukaryotic intracellular catalase-peroxidases

(Catalase-peroxidase from *Magnaporthe grisea*)

Master Thesis

Performed at the

Department of Chemistry – Division of Biochemistry

BOKU – University of Natural Resources and Life Sciences, Vienna

Submitted by

Marcus Motz

2014

Table of contents

1. Abstract

Catalase-peroxidases (KatGs) are bifunctional heme-*b* containing metalloenzymes which accomplish both catalase (2 H_2O_2 → 2 H_2O + O_2) and peroxidase reaction (H_2O_2 + 2 AH_2 → 2 H_2O + 2 $HA^{\bullet}$) within a single active site. In eukaryotes, there are two groups of KatGs namely intracellular and extracellular catalase-peroxidase (KatG1 and KatG2, respectively). This work deals with the intracellular catalase-peroxidase derived from *Magnaporthe grisea* (MagKatG1). Expression of MagKatG1 was performed in *Escherichia coli* and purification of the His-tagged protein was done with metal chelate affinity chromatography (MCAC) and hydroxyapatite chromatography (HAC). Characterization was done via electrophoresis and Coomassie Brilliant Blue staining and immunodedection. Kinetic parameters were determined photometrically with a UV/VIS-spectrophotometer (Hitachi, steady-state kinetics) and a stopped-flow apparatus (Applied Photophysics, steady-state and pre-steady-state kinetics). Investigation of the reaction scheme, which is studied best for bacteria, and determination of rate constants as well as spectral characteristics were done for the reaction from ferric enzyme to Compound I (a ferryl enzyme state) and back with hydrogen peroxide (H_2O_2), peroxyacetic acid (PAA) and hypochlorite (OCl^-). MagKatG1 shows catalase activity and peroxdase activity (for guaicacol) of 27 and 0.013 Units mg^{-1} enzyme, respectively. Compound I-formation was performed with peroxyacetic acid and hypochlorite and the rate constants are 1.2×10^4 M^{-1} s^{-1} and 2×10^6 M^{-1} s^{-1}, respectively. The rate constant for PAA is similar to the rate constant of SynKatG. Reaction with hypochlorite showed two intermediates, so three very similar rate constants were determined for the back reaction to ferric enzyme: $1.2 - 1.3 \times 10^4$ M^{-1} s^{-1}. All results are discussed in comparison to KatG of *Synechocystis*.

2. Abstract Deutsch

Katalase-Peroxidasen (KatGs) sind Metalloenzyme, die Häm-*b* enthalten, und 2 verschiedene Reaktionen vollziehen können, nämlich die Katalasereaktion ($2\ H_2O_2 \rightarrow 2\ H_2O + O_2$) und Peroxidaseraktion ($H_2O_2 + 2\ AH_2 \rightarrow 2\ H_2O + 2\ HA^{\bullet}$) innerhalb eines aktiven Zentrums. Zwei unterschiedliche KatG-Gruppen wurden bisher in Eukaryonten gefunden: intrazelluläre und extrazelluläre Katalase-Peroxidasen (KatG1 bzw. KatG2). Diese Arbeit beschäftigt sich mit der intrazellulären Katalase-Peroxidase von *Magnaporthe grisea* (MagKatG1). Exprimiert wurde MagKatG1 in *Escherichia coli*, die Aufreinigung des His-Tag Proteins erfolgte mittels Metallchelataffinitätschromatographie (MCAC) und Hydroxyapatitchromatographie (HAC). Die Charakterisierung wurde mit Elektrophorese und anschließende Färbung mit Coomassie Brilliant Blue und Immunodetektion durchgeführt. Die kinetischen Parameter wurden photometrisch mit einem UV/Vis-Spektrophotmeter (Hitachi, steady-state-Kinetik) und mit einem Stopped-Flow Gerät (Applied Photophysics, steady-state- und pre-steady-state-Kinetik) bestimmt. Der Reaktionsmechanismus, welcher am besten für bakterielle KatGs untersucht ist, die Bestimmung der Geschwindigkeitskontanten sowie spezielle Eigenschaften der Spektren wurden für die Reaktionen vom Grundzustand (Fe(III)-Enzym) zum Compound I (Fe(IV)-Enzym) und die Rückreaktionen erforscht, wobei folgende Substrate eingesetzt wurden: Wasserstoffperoxid (H_2O_2), Peroxyessigsäure (PAA) und Hypochlorit (OCl^-). MagKatG1 besitzt eine Katalaseaktivität von 27 Units mg^{-1} Enzym und eine Peroxidaseaktivität (Guaiacol als Substrat) von 0.013 Units mg^{-1} Enzym. Die Geschwindigkeit der Bildung von Compound I beträgt mit PAA $1.2 \times 10^4\ M^{-1}\ s^{-1}$ und mit OCl^- $2 \times 10^6\ M^{-1}\ s^{-1}$. Die Geschwindigkeitskonstante für PAA ist vergleichbar mit der von SynKatG. Die Reaktion mit Hypochlorit zeigte zwei Intermediate, sodass drei Geschwindigkeitskonstanten für die Rückreaktion zum Fe(III)-Enzym bestimmt wurden, die zwischen $1.2 – 1.3 \times 10^4\ M^{-1}\ s^{-1}$ liegen. Alle Ergebnisse werden im Vergleich zur KatG von *Synechocystis* diskutiert.

3. Introduction

Degradation of hydrogen peroxide (H_2O_2), which represents the most abundant reactive oxygen species (ROS), is of essential importance for prokaryotic, eukaryotic cells and for some anaerobic bacteria. This degradation of H_2O_2 can be done by its reduction to water with the help of endogenous electron donors, but more efficiently by metalloenzyme-mediated dismutation to dioxygen (O_2) and water. Evolution led to three metalloenzyme families namely typical (monofunctional) heme catalases (KatEs), bifunctional catalase-peroxidases (KatGs) and non-heme manganese catalases (MnCats). KatGs are able to accomplish the peroxidase reaction ($H_2O_2 + 2\ AH_2 \rightarrow 2\ H_2O + 2\ HA^{\bullet}$) as well as the catalase reaction (H_2O_2 dismutation, $2\ H_2O_2 \rightarrow 2\ H_2O + O_2$). Phylogenetic analyses were done for all three catalatically active enzyme families. [M. Zamocky, 2012a]

3.1. Phylogeny of monofunctional heme catalases, bifunctional catalase-peroxidases and non-heme manganese catalases

3.1.1. Typical (monofunctional) heme catalases

KatEs can be found among bacteria, archaea and eukarya. The phylogenetic tree consists of three main clades of the catalase superfamily including large subunit catalases (Clade 2, about 750 residues per subunit) and small subunit catalases (Clade 1 and 3, about 500 residues per subunit). All of the compared enzymes hold for a high conservation, organization and architecture of the typical catalase fold as about 460 residues are highly conserved. Evolution started with large subunit catalases (Clade 2) comprising bacterial and fungal enzymes whereas ancestors of these are located in the basal branch. Further steps led through proteobacterial large subunit enzymes, to Bacteroidetes, which possess genes for both monofunctional catalases and bifunctional catalase-peroxidases, to fungal extracellular group (having a predicted signal sequence for secretion) and finally to the fungal intracellular group whereas both fungal groups originate from pathogenic fungi. Obviously, small subunit catalases (Clade 1 and 3) evolved from ancestral Clade 2 catalases but all known representatives have lost the C-terminal domain (flavodoxin-like domain) and some further evolved proteins have a fused lipoxygenase domain. Proteobacterial, plant, worm or mammalian catalases can be found within these two clades, just to mention a few. [M. Zamocky, 2012a]

3.1.2. (Bifunctional) catalase-peroxidases

KatGs belong to the Class I of the peroxidase-catalase superfamily, which contains homologous cytochrome *c* peroxidases, ascorbate peroxidases and hybrid type peroxidases. Evolution of the peroxidase-catalase superfamily started with proteins that possess two domains per subunit, the N-terminal heme-containing domain and the C-terminal domain without a cofactor. Extant catalase-peroxidases are able to accomplish a peroxidase reaction as well as a significant (pseudo-) catalase activity that differs mechanistically from the classical catalatic reaction of typical catalases but still follows the reaction 2 H_2O_2 → 2 H_2O + O_2. Later on in evolution of the peroxidase-catalase superfamily the C-terminal domain was lost and all further representatives of this heme peroxidase superfamily are typical (monofunctional) peroxidases that have lost the ability of H_2O_2 dismutation.

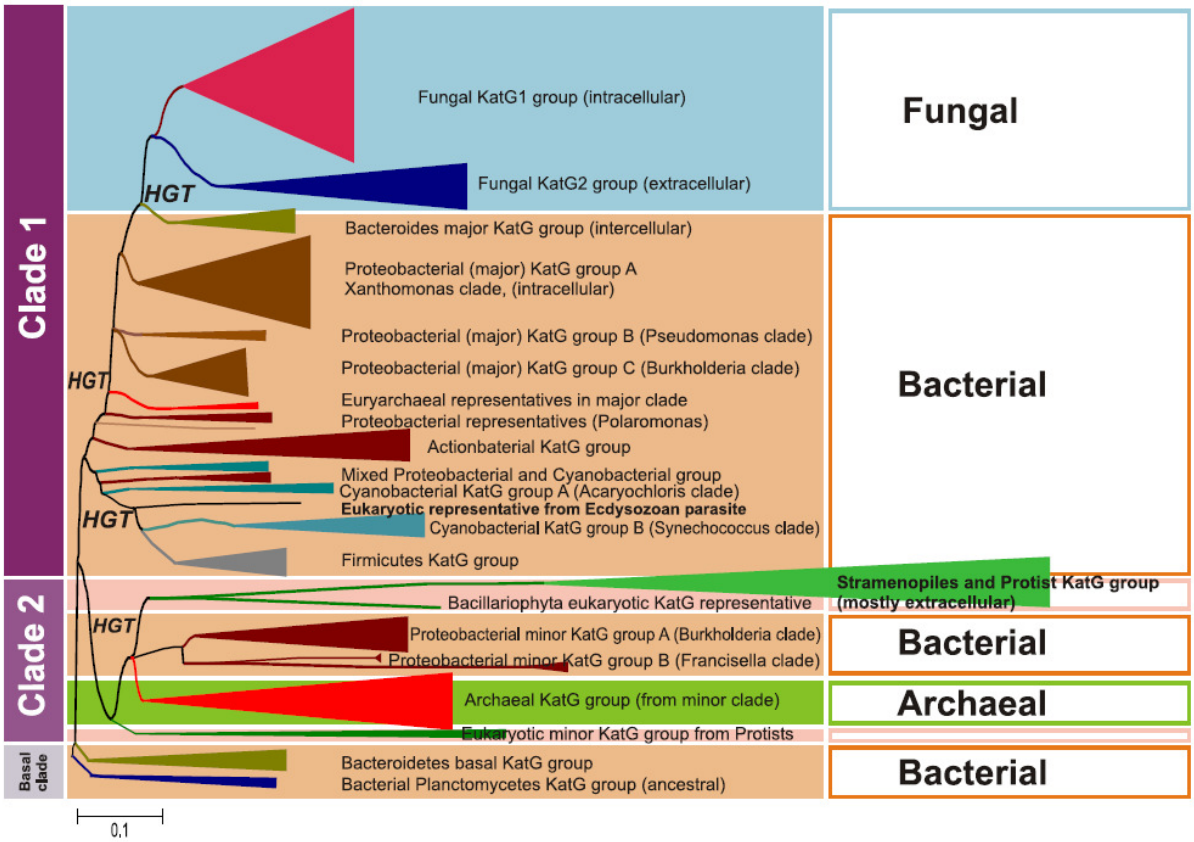

Figure 1: *Overview of an unrooted tree of 204 catalase-peroxidases obtained with the Maximum Likelihood method of the MEGA package. [M. Zamocky, 2012a]*

Full-length KatG sequences (204) from archaea, bacteria and lower eukaryotes were taken for phylogenetic analyses. Reconstruction (see Figure 1) reveals a clear distinction between two basic paralog clades, namely main Clade 1 and minor Clade 2.

The origin of *katG* gene was located in the clade of marine heterotrophic bacteria from the phylum Planctomycetes having the KatG from cyanobacterium *Gloeobacter violaceus* as the closest phylogenetic neighbor. Gloeobacteria might represent the closest extant of primordial cyanobacteria that did not possess thylakoid membranes. Maybe after *katG* acquisition by *Gloeobacter* was able to react on photooxidative stress. There is a close connection between ancestral Planctomycetes and a homogenous basal branch containing only sequences from Bacteroidetes. In Clade 1 KatGs from Cyanobacteria and Firmicutes segregated very early. Interestingly, one single eukaryotic representative, *Lepeoptherius salmonis*, shows sequence similarities typical for eubacterial catalase-peroxidases.

Further steps of evolution led to branches of Actinobacteria, Proteobacteria (major groups A, B and C) as well as euryarchaeal representatives. The proteobacterial group includes e.g. KatGs from phytopathogens (*Xanthomona*s) or endophytes (e.g. *Burkholderia phytofirmans*).

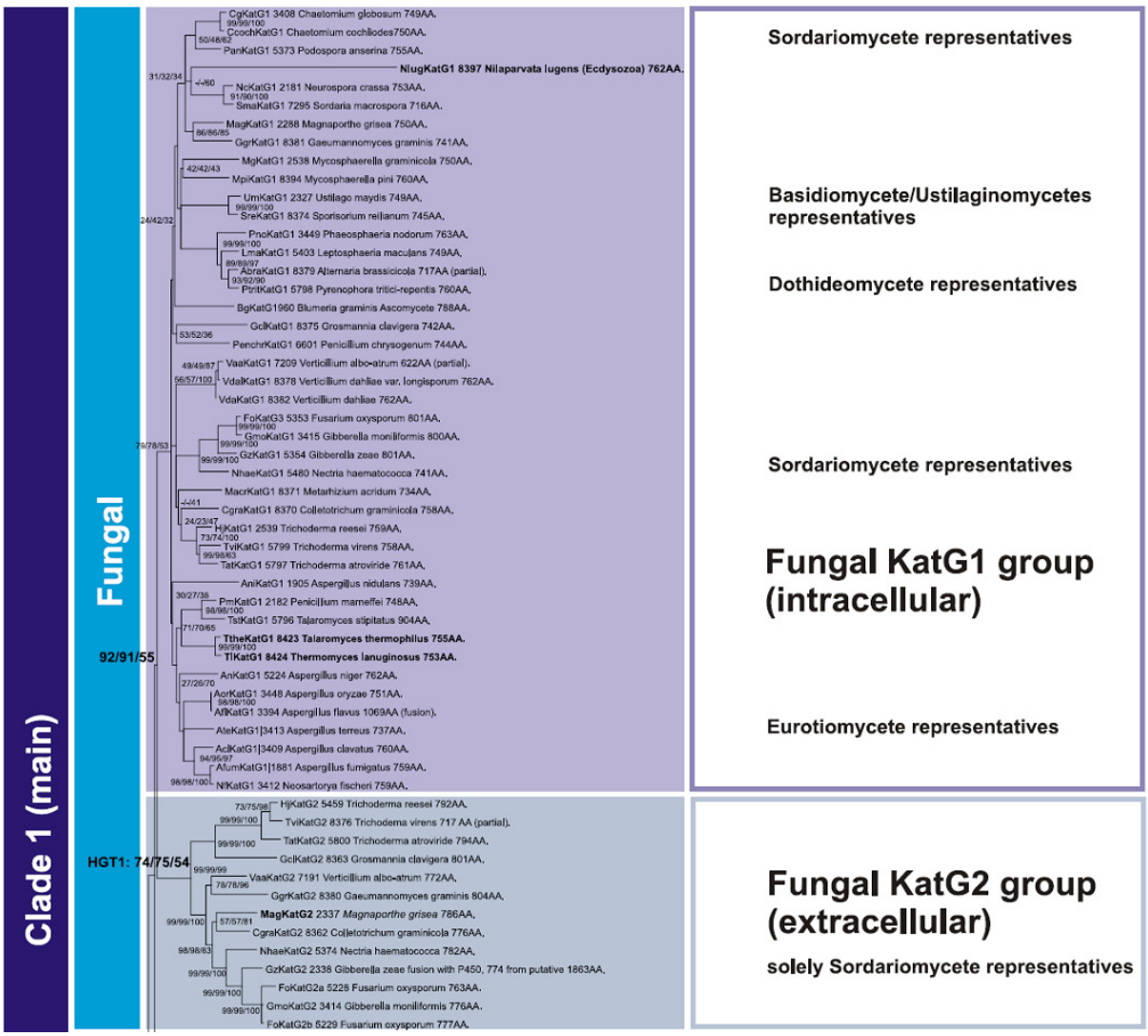

Figure 2: *Detailed list of catalase-peroxidases forming intracelluar and extracellular fungal KatG groups. [M. Zamocky, 2012a]*

A major horizontal gene transfer (HGT) event between Bacteroidetes and an ancestor of the sac fungi led to the fungal KatGs. After ancestral ascomycetes acquired *katG* sequences the occurrence of a gene duplication led to the divergence of intracellular KatG1 (more abundant) and extracellular KatG2 groups (see Figure 2).

Further steps led to subgroups of Eurotiomycetes and Sordariomycetes catalase-peroxidases, which have a peroxisomal targeting signal (PTS1 signal) and are most likely located in peroxisomes and a further HGT towards Basidiomycetes occurred. Compared to KatG1, all representatives of fungal KatG2 groups have an N-terminal signal sequence for secretion and all *katG2* genes originate from Sordariomycetes. Extracellular KatG is in case of the rice blast fungus *Magnaporthe grisea* essential to overcome the oxidative burst and release of hydrogen peroxide as a countermeasure.
Catalase-peroxidases of Clade 2 separated from Clade 1 rather early and contain the following KatG groups: Protists / Oomycetes group, Euryarchae minor group, proteobacterial minor group and minor protozoan group. [M. Zamocky, 2012a]

3.1.3. Manganese (non-heme) catalases

To complete the phylogeny of metalloenzyme family evolution of MnCats has to be mentionend as well. These proteins possess only a single domain with a typical ferritin-like four helical bundle and belong to a complex (ferritin-like) superfamily. 100 full length protein sequences reveal five distinct clades, a basal clade and a clade which connects the basal clade and clades one to five. An important step in the evolution of manganese catalases was a gene duplication, which separates Clade 1-3 from Clades 4-5. All clades contain bacterial and archaeal proteins and so far no eukaryotic representative is found. This suggests that MnCats are the oldest enzymes for hydrogen peroxide dismutation. [M. Zamocky, 2012a]

3.2. Magnaporthe grisea

The phytopathogenic ascomycete *M. grisea* is the cause for the disease rice blast. Additionally, different forms of *M. grisea* also infect a broad range of grass species such as wheat and barley. The life cycle including infection and reproduction can be seen in Figure 3. Once the phytopathogen has infected a host cell, an appressorium is developed to invade and create lesions. Sexual reproduction only occurs when two strains of opposite mating type meet, otherwise asexual reproduction is chosen.

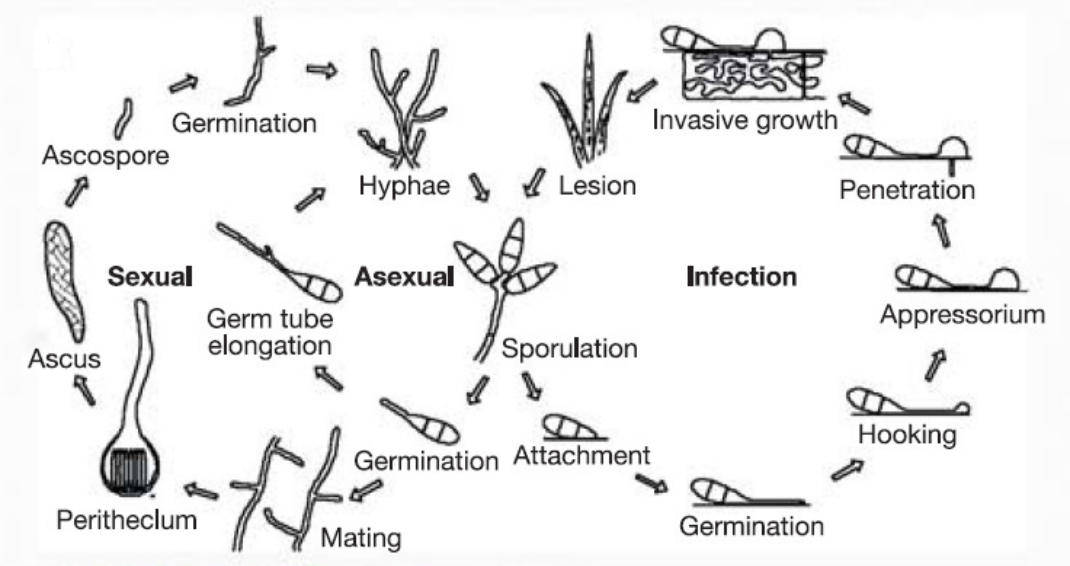

Figure 3: *Life cycle of Magnaporthe grisea. Asexuell spores called conidia germinate and develop a specialized infection structure, the appressorium. Invasive growth within and between cells culminates with sporulation and lesion formation. Sexual reproduction occurs when two strains of opposite mating type meet and form a perithecium in which ascospores develop. Once released, ascospores can develop appressoria and infect host cells. [R. A. Dean, 2005]*

The total length of the draft genome is 37.9 Mb and 11109 genes were predicted with protein products of longer than 100 amino acids. Compared to other fungi (10082 for *Neurospora crassa* and 9457 for *Aspergillus nidulans*, both non-pathogenic), *M. grisea* possesses more genes which suggests that these additional genes may have an input on the pathogenicity. To be a successful pathogen, the plant's innate immune system has to be suppressed and host metabolism and cell signaling must be disturbed to promote fungal growth.

M. grisea has the largest number (among sequenced fungi) of CFEM-GPCR-like proteins (G-protein-coupled receptors that contain a conserved fungal-specific extracellular membrane-spanning domain), which are expressed during the cycle of infection. GPCRs transduce environmental signals and activate second messengers and regulate gene expression. Furthermore, three mitogen-activated protein kinase (MAPK) cascades were located that regulate appressorium development, penetration peg formation and adaption to hyper-osmotic stress whereas two of this three MAPK pathways control virulence-associated development. Additionally, cyclic AMP plays a role in the formation of appressorium and the turgor-driven process. The high turgor pressure needed is achieved by accumulation of glycerol. Glycerol may be synthesized either from storage products or glycolytic intermediates (dihydroxyacetone phosphate and dihydroxyacetone) and may be performed

both in mitochondria and in catalase-free glyoxysome-like bodies. Several of putatively secreted proteins are predicted to degrade the plant cell wall and cuticule.

The plant adaptive immune system has evolved to recognize pathogen effector proteins (called pathogen-associated molecular patterns, PAMPs) that are regulated by a gene-for-gene system. Another countermeasure of plants is the release of reactive oxygen species (ROS) such as hydrogen peroxide during plant-pathogen interaction. *M. grisea* possesses two enzymes to deal with this oxidative burst: intracellular (KatG1) and extracellular (KatG2) catalase-peroxidase. [R. A. Dean, 2005]

3.3. Catalase-peroxidases

Catalase-peroxidases (KatGs, EC 1.11.1.21) are bifunctional non-animal heme *b* containing peroxidases (oxidoreductases) and belong to Class I of the peroxidase-catalase superfamily including homologous cytocrome *c* peroxidases (C*c*P), ascorbate peroxidases (APx) and hybrid-type peroxidases. Representatives of Class II are fungal lignin and manganese peroxidases and secretory plant peroxidases related to horseradish peroxidase (HRP) are found in Class III. KatGs are homodimers with each subunit contained of N- and C-terminal domains but only the N-terminal domain possesses a heme cavity that is very similar to that of C*c*P and APx.

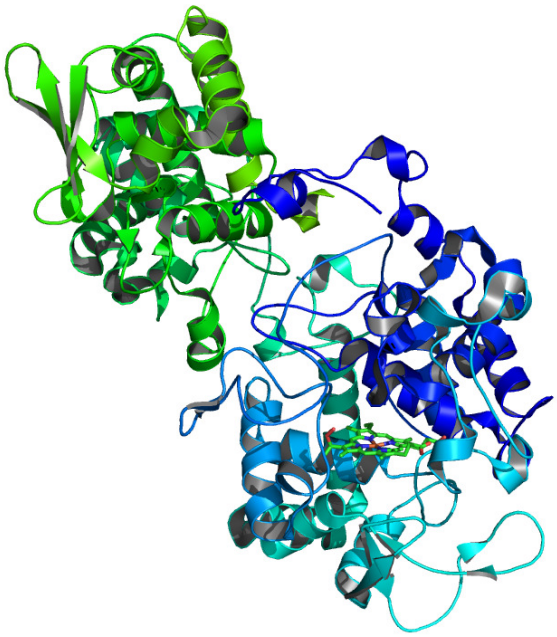

Figure 4: *Crystal structure of catalase-peroxdidase from Burkholderia pseudomallei. This is the closest homologous structure compared to the KatG1 from M. grisea (so far, no crystal structure of MagKatG1 but the crystal structure of MagKatG2 is*

available). The figure shows one monomer that contains two domains: the N-terminal domain in blue (catalytically active) which possesses the prosthetic group and the C-terminal domain in green. Protein code (1MWV) taken from NCBI/PubMed and viewed with Pymol [The PyMOL Molecular Graphics System, Version 1.3 Schrödinger, LLC.]

In fungi, two distinct groups have been identified, namely intracellular (KatG1 – present in both non-pathogenic and pathogenic fungi) and extracellular (KatG2 – only found in phytopathogenic fungi) KatGs. KatG1 holds high structural and functional similarities to their bacterial counterparts (see Figure 4 and Figure 5) and all representatives of extracellular group have an N-terminal sequence - of about 20 amino acids - for protein secretion that is also found in bacterial KatGs but not in Bacteroidetes. This suggests that the signal sequence (specific for ascomycetes) has been acquired later in evolution. [J. Vlasits, 2010a, M. Zamocky, 2009a, 2010, 2012a, 2012b, 2012c]

3.4. Intracellular catalase-peroxidase from *M. grisea*

Multiple sequence alignments (36 fungal and 13 bacterial KatGs) show highly conserved regions along the whole genetic code (including the active site around the heme) [M. Zamocky, 2009a]. On the distal side of the prosthetic heme group, the catalytic triad Arg^{87} – Trp^{90} – His^{91} (*M. grisea* KatG1 numbering) is strictly conserved. These investigated protein sequences show the presence of Asn^{121}, which is the hydrogen-bonding partner of distal His^{91}, Asp^{120}, that controls the access of hydrogen peroxide to the active site and the KatG-typical covalent adduct Trp^{90} – Tyr^{238} – Met^{264}, which is crucial for the catalase activity. On the other side, the proximal side shows the triad His^{279} – Trp^{330} – Asp^{389} that is fully conserved in both groups of fungal KatGs. So far, it was not possible to receive a crystal structure of intracellular catalase peroxidase from *M. grisea*. [M. Zamocky, 2009a]

Figure 5 shows a 3D-model of MagKatG1 monomer in overlay with the known structure of KatG from *B. pseudomallei*. Calculations resulted in similar bond lengths and angles as well as the typical conserved distal (Arg^{87} – Trp^{90} – His^{91}) and proximal (His^{279} – Trp^{330} – Asp^{389}) triads within the active site. Furthermore, the KatG-typical amino acids Tyr^{238} and Met^{264} are shown, which are covalently linked to the distal Trp^{111}. All these mentioned amino acids are strictly conserved in prokaryotic and eukaryotic KatGs. [M. Zamocky, 2009b]

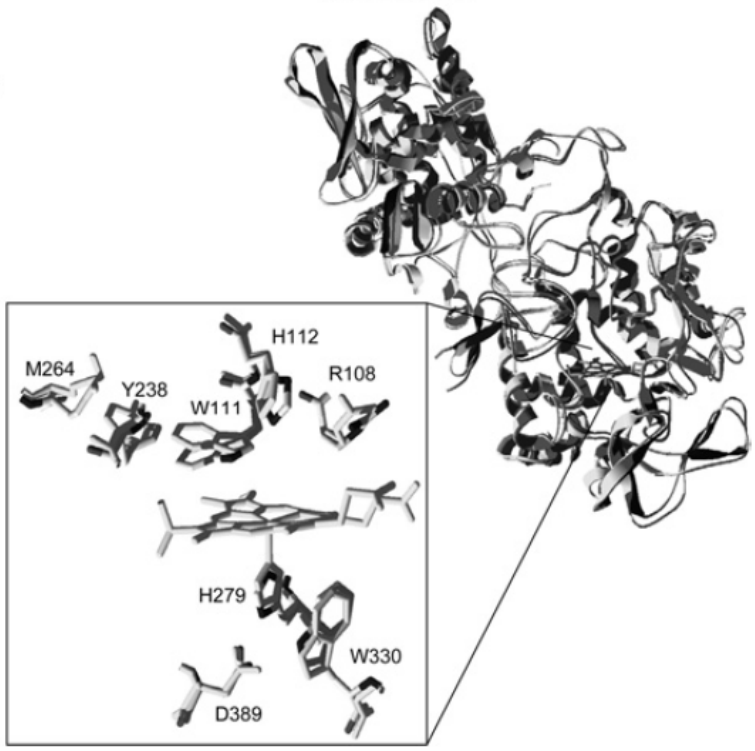

Figure 5: *Homology model of the 3D structure of MagKatG1 monomer. An overlay with the known structure of KatG from B. pseudomallei is presented. [M. Zamocky, 2009b]*

Magnaporthe grisea expresses intracellular MagKatG1 constitutively, in comparison to extracellular MagKatG2. This was documented by experiments where cultures of *M. grisea* were grown in the absence and presence of hydrogen peroxide or peroxyacetic acid or paraquat. It is assumed that MagKatG1 degrade H_2O_2 continuously and MagKatG2 is produced during oxidative stress conditions (significantly enhanced expression under oxidative stress conditions). [M. Zamocky, 2009b]

3.5. Reaction mechanism

Hydrogen peroxide is a reactive oxygen species (ROS) and is formed by either oxidoreductases or by dismutation of superoxide or by auto-oxidation of biomolecules. Degradation of this ROS can be done enzymatically by its reduction to water or by dismutation to O_2 and water ($2\ H_2O_2 \rightarrow 2\ H_2O + O_2$). [M. Zamocky, 2012a]

Figure 6 shows reactions to be accomplished by either monofunctional catalases, peroxidases or catalase-peroxidases. In general, hydrogen peroxide reacts with ferric states, Fe(III), of heme-containing peroxidases (EC 1.11.1.7) and catalases (EC 1.11.1.6) in a two-electron redox reaction whereas the O-O bond is cleaved heterolytically and leads to an intermediate called Compound I, an oxyferryl state Fe(IV)=O (see Figure 6), as the radical is located at the porphyrin ($Por^{\bullet+}$).

Reaction (1): $[aa\ Fe(III)\ Por] + H_2O_2 \rightarrow [aa\ Fe(IV)=O\ Por^{\bullet+}] + H_2O$

Compound I can be transformed into Compound I* moving the radical to the protein matrix [$aa^{\bullet+}$ Fe(IV)-OH Por]. The two mentioned Compounds are deficient of two electrons and in heme peroxidases reduction can be done either by two one-electron reduction steps (Reaction (2) and (3)) or one two-electron reduction step (Reaction (4)).

Reaction (2): $[aa\ Fe(IV)=O\ Por^{\bullet+}] + AH \rightarrow [aa\ Fe(IV)\text{-}OH\ Por] + A^{\bullet+}$

Reaction (3): $[aa\ Fe(IV)\text{-}OH\ Por] + AH \rightarrow [aa\ Fe(III)\ Por] + H_2O + A^{\bullet+}$

Reaction (4): $[aa\ Fe(IV)=O\ Por^{\bullet+}] + X^- \rightarrow [aa\ Fe(III)\ Por] + H_2O + HOX$

Monofunctional heme catalases use a second hydrogen peroxide molecule for reduction of Compound I and the release of dioxygen (Reaction (5)).

Reaction (5): $[aa\ Fe(IV)=O\ Por^{\bullet+}] + H_2O_2 \rightarrow [aa\ Fe(III)\ Por] + H_2O + O_2$

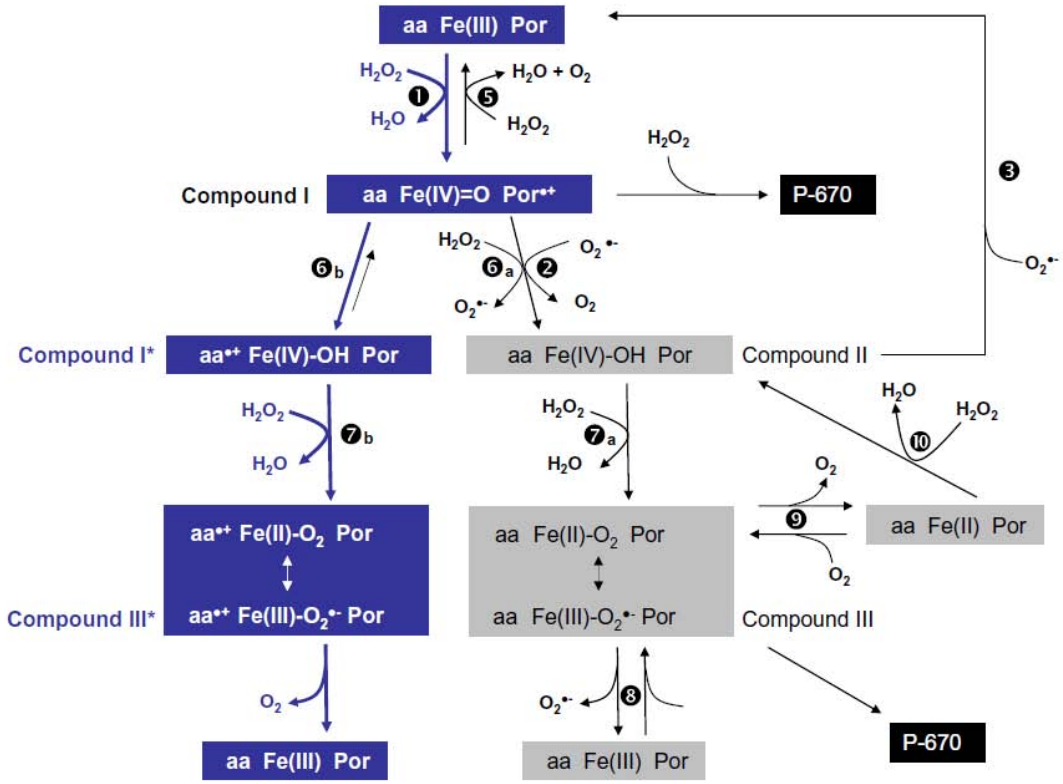

Figure 6: *Reaction scheme for monofunctional catalases, peroxidases and KatGs. Reaction intermediates formed upon incubation of heme peroxidases with excess of hydrogen peroxide and in the absence of exogenous electron donors. Hydrogen peroxide dismutation by monofunctional catalases follows Reaction (1) and (5). Peroxidases show a pseudo-catalase activity following the reaction sequence ferric enzyme → Compound I → Compound II → Compound III → ferric enzyme. By contrast, KatGs are proposed to follow the reaction sequence ferric enzyme → Compound I → Compound I* → Compound III* → ferric enzyme (pathway highlighted in blue). [J. Vlasits, 2010a].*

3.5.1. Heme peroxidases

The oxidant H_2O_2 is also an inactivating agent of metalloproteins such as peroxidases. As a consequence, with large excess of hydrogen peroxide and in the absence of exogenous electron donors heme peroxidases are irreversibly inhibited with time. This process is indicated by an absorption band at 940 nm (P-940) and a further decay leads to a peak at 670 nm (verdohemoprotein, P-670). In the presence of exogenous electron donors there is a competition for Compound I between the electron donor and H_2O_2.

Inactivation and formation of P-670 requires specific intermediates and hydrogen peroxide. Formation of Compound I (Reaction (1)) is followed by formation of Compound II and

Compound III (slowly decays to ferric enzyme) whereas a fraction of enzyme is irreversibly converted to P-670. Reaction (6a) and (7a) show the reaction of Compound I with H_2O_2 and Compound II with H_2O_2.

Reaction (6a): $[aa\ Fe(IV)=O\ Por^{\bullet+}] + H_2O_2 \rightarrow [aa\ Fe(IV)\text{-}OH\ Por] + O_2^{\bullet-} + H^+$

Reaction (7a): $[aa\ Fe(IV)\text{-}OH\ Por] + H_2O_2 \rightarrow [aa\ Fe(II)\text{-}O_2\ Por] + H_2O + H^+$
$\leftrightarrow [aa\ Fe(III)\text{-}O_2^{\bullet-}\ Por]$

To avoid this Reaction (6a) which seems to be absent or extremely inefficient in most peroxidases, the porphyryl radical can migrate to an amino acid of the protein moiety Reaction (6b) and can be an unphysiological side reaction (slow in most peroxidases but much faster in e.g. catalase-peroxidases). Resulting Compound I* further reacts with hydrogen peroxide to Compound III* (Reaction (7b)).

Reaction (6b): $[aa\ Fe(IV)=O\ Por^{\bullet+}] + H^+ \rightarrow [aa^{\bullet+}\ Fe(IV)\text{-}OH\ Por]$

Reaction (7b): $[aa^{\bullet+}\ Fe(IV)\text{-}OH\ Por] + H_2O_2 \rightarrow [aa^{\bullet+}\ Fe(II)\text{-}O_2\ Por] + H_2O + H^+$
$\leftrightarrow [aa^{\bullet+}\ Fe(III)\text{-}O_2^{\bullet-}\ Por]$

Reaction (7a) and (7b) describe the reaction of Compound II or Compound I* with H_2O_2 as a two-electron reductant forming dioxygen that remains bound to the heme iron. This Compound III or Compound III* is a ferrous-dioxygen/ferric superoxide complex. Compound III is relatively stable and has two options for decay, either to the ferric (Reaction 8) or to the ferrous state (Reaction 9). Ferrous peroxidase either recombines with O_2 forming Compound III (Reaction 9) or reacts with H_2O_2 forming Compound II (Reaction10)

Reaction (8): $[aa\ Fe(II)\text{-}O_2\ Por] \leftrightarrow [aa\ Fe(III)\text{-}O_2^{\bullet-}\ Por] \leftrightarrows [aa\ Fe(III)\ Por] + O_2^{\bullet-}$

Reaction (9): $[aa\ Fe(II)\text{-}O_2\ Por] \leftrightarrow [aa\ Fe(III)\text{-}O_2^{\bullet-}\ Por] \leftrightarrows [aa\ Fe(II)\ Por] + O_2$

Reaction (10): $[aa\ Fe(II)\ Por] + H_2O_2 \rightarrow [aa\ Fe(IV)\text{-}OH\ Por] + H_2O$

The above described reaction steps (ferric enzyme → Compound I → Compound II → Compound III → ferric enzyme according Reaction (1), (6a), (7a) and (8)), can be observed in peroxidases and are often designated as catalase like or pseudo-catalatic activity.

3.5.2. Catalase-peroxidases

In catalase-peroxidases it was shown that mutations of any residue of the Met-Tyr-Trp adduct, which are covalently linked together, affects the catalase activity. Catalase-peroxidases form a special oxyferrous heme (Compound III-like) in the presence of high concentrations of H_2O_2 (similar to monofunctional peroxidases in the presence of H_2O_2 and absence of electron donor). This heme state seems to be highly unstable due to rapid cycling while this form exists. Suggesting that one cycle of H_2O_2-dismutation includes at least one two-electron oxidation step of hydrogen peroxide because both oxygen atoms of dioxygen are derived from one molecule of H_2O_2. [J. Vlasits, 2007] Another peculiarity is the forming of protein radicals, which means the movement of the radical site from the porphyrin into the protein (see Reaction (6), Figure 6), which influences either the catalase or the peroxidase reaction depending on the location of the radical. It has been demonstrated that the radical only persists during turnover of hydrogen peroxide and was mainly found on the oxygen of tyrosyl moiety of the oxidized Met-Tyr-Trp adduct and shows the participation of the KatG-typical covalent adduct in the reaction of ferric enzyme with H_2O_2.

For catalase-peroxidases, the reaction mechanism follows the same pathway as in monofunctional peroxidases with the exception of modified electronic structures (blue pathway, see Figure 6). KatG reacts with hydrogen peroxide to Compound I (Reaction (1)), which is very unstable, and is rapidly converted to Compound I* (Reaction (6b)). Compound I* further reacts with H_2O_2 to an oxyferrous heme state (Compound III*, Reaction (7b)) that is in equilibrium with superoxide bound to ferric enzyme, whereas this intermediate is rapidly converted into ferric enzyme and dioxygen. [J. Vlasits, 2010a]

4. Aims of investigation

Prokaryotic catalase-peroxidases of prokaryotes (e. g. *Synechocystis*) have been investigated and studied best, and the reaction mechanism is available for SynKatG. So far, fungal KatGs have hardly been investigated. Expression, purification and biochemical characterization for both intracellular and extracellular KatG from *Magnaporthe grisea* had been stated [M. Zamocky, 2012b] and recently the structure of MagKatG2 was clarified. Neither the structure nor the reaction mechanism for MagKatG1 could be resolved up to know.

Expression of intracellular catalase-peroxidase derived from *Magnaporthe grisea* (MagKatG1) was performed in *E. coli* and purified with metal chelate affinity chromatography (MCAC) and hydroxyapatite chromatography (HAC) according to the procedure published by Zamocky et.al. [M. Zamocky, 2009b]

The reaction mechanism described above, which was derived for bacterial KatGs (in this case: *Synechocystis* KatG, [J. Vlasits, 2010a]) serves as a model for the performed experiments with eukaryotic intracellular KatG (MagKatG1) to determine the reaction mechanism and the kinetic parameters. The scope of this work was to investigate the Compound I-formation and -reduction (Reaction (1) and (5) shown in Figure 6) with different substrates like peroxyacetic acid (PAA), hypochlorous acid (HOCl), and hydrogen peroxide (H_2O_2). By comparison of eukaryotic and bacterial KatGs it will be possible to figure out all similarities or differences in their reaction mechanism and furthermore these experiments could serve as a basis for further investigations of the reaction mechanism of intracellular eukaryotic catalase-peroxidases.

To sum up, the aims of this work were the expression, purification and characterization of MagKatG1 and furthermore the kinetic determination of the rate constants and the corresponding spectral changes for the reactions with different substrates.

5. Material and Methods

The *katG1* gene was amplified from cDNA of *Magnaporthe grisea* (synonym *Pyricularia grisea*). The organism was obtained from the culture collection of University of Natural Resources and Life Sciences in Vienna. A hexa-histidine tag has been C-terminally fused to the gene and then it was inserted in a pMZM1 vector as shown in Figure 7. Finally, the enzyme was expressed heterologously in *Escherichia coli* BL21 (DE3*) in high amounts, with high purity and almost 100% heme occupancy as described by Zamocky et al. [M. Zamocky, 2009b]

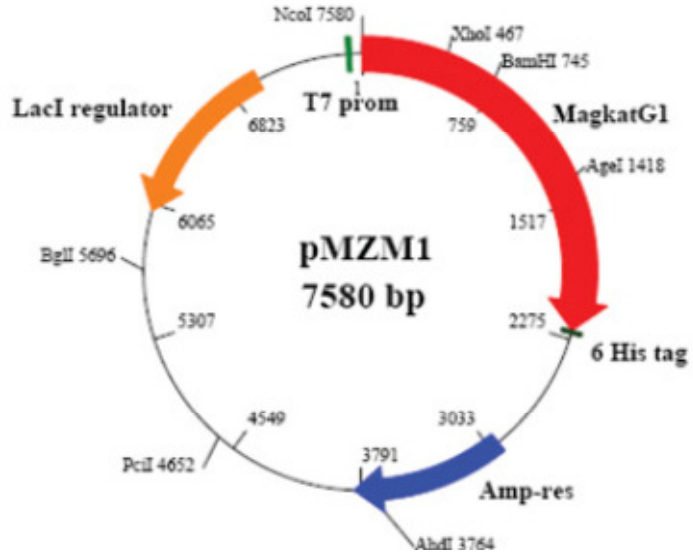

Figure 7: *Recombinant plasmid used for the heterologous expression of the MagKatG1 gene (shown in red, ligated into pET21d vector). [M. Zamocky, 2009b]*

5.1. Expression of KatG in *E. coli* BL21 (DE3*)

12 mL LB_{Amp}-medium was inoculated with a preparatory culture and incubated over night at 37 °C and shaking (180 rpm). 1 L of $M9ZB_{Amp}$-medium (see the composition below) was inoculated with 12 mL of the prepared LB_{Amp}-culture. The inoculated $M9ZB_{Amp}$-medium was incubated at 37°C until the OD_{600} reached the value of 0.9 – 1.1.

Heterologous expression was achieved at 16°C and addition of hemin (8.3 µM final concentration) and IPTG (1 mM final concentration) to the $M9ZB_{Amp}$-medium (cultivation

medium – see composition below) for 16 h and shaking at 180 rpm. Solutions A to D were autoclaved separately.

The bacterial suspension was centrifuged at 6000 rpm for 15 min; the pellet was resuspended and transferred into Falcon tubes. Another centrifugation step was performed at 3000 rpm for 20 min. The supernatant was discarded and the cell pellet was used for purification steps or stored at -20°C.

Material:

Composition of $M9ZB_{Amp}$-Medium (ca. 1 L):

800 mL Solution A + 100 mL Solution B + 100 mL Solution C + 1 mL Solution D + 1 mL Ampicillin solution

Solution A: (per 1 L Medium)
20 g pepton
10 g yeast extract
5 g NaCl (M_r = 58.44 g/mol)
1 g NH_4Cl (M_r = 53.49 g/mol)
Add 800 mL RO-H_2O

Solution B: 12 g KH_2PO_4 (M_r = 136.1 g/mol)
24 g Na_2HPO_4 (M_r = 268 g/mol)
Add 400 mL RO-H_2O

Solution C: 16 g Glucose (M_r = 180.16 g/mol)
Add 400 mL RO-H_2O

Solution D: 12.3 g $MgSO_4*7H_2O$ (M_r = 246.48 g/mol)
Add 50 mL RO H_2O

Ampicillin: 100 mg Na-Ampicillin per 1 mL H_2O
Sterile filtration and stored at -20°C

Equipment:

Centrifuge: Sorvall Instruments RC5 or RC6

Rotor: SLA-3000

5.2. Cell lysis and Metal-Chelate-Affinity-Chromatography (MCAC)

All steps were performed on ice. The cell pellet was either used directly or thawed, resuspended in buffer A and 3 protease inhibitors were added: leupeptin (1:500 v/v), pepstatin (1:500 $^{v}/_{v}$), phenylmethylsulfonyl fluoride (PMSF, 1:1000 $^{v}/_{v}$). Homogenization was performed by four ultrasonication steps (length of each step was 40 seconds, pulser 50%, intensive cooling was done between the steps). Then the crude homogenate was centrifuged for 20 min at 18000 rpm.

The pellet was discarded and the cleared supernatant was taken for MCAC. The chelating sepharose fast flow column was loaded with Ni^{2+}-ions and afterwards washed with100 mL of buffer A. Bound protein was eluted with a linear gradient of buffer A to 100% of buffer B. The flow rate varied from 1.5 – 2.5 mL per min and the fraction volume varied from 2.5 – 4 mL.
After elution of the protein, the column was washed with 50 mM EDTA pH 8.0 until all Ni^{2+}-ions were washed away. Regeneration of the gel was performed by washing with 50 mL of distilled water and 50 mL of ethanol (20%), which represents storage conditions.

The collected in fractions were analysed spectrometrically in order to estimate the protein content and the catalase activity.

<u>Material:</u>

Buffer A: 50 mM phosphate buffer + 100 mM NaCl at pH 8.0
Buffer B: 50 mM phosphate buffer + 100 mM NaCl + 500 mM Imidazole at pH 7.6
Gel: Chelating Sepharose Fast Flow (GE Healthcare)

<u>Equipment:</u>

Ultrasonication device: Vibra-Cell, type CV17
Centrifuge: Sorval Instruments, RC5 or RC6,
Rotor: SS-34
Peristaltic Pump
Fraction collector
Gradient mixer (Biorad)
Membrane vacuum pump

5.3. Ultrafiltration and desalting

Ultrafiltration was done with Amicon Centriprep 30 and centrifugation was performed for 20 min at 2500 rpm at 4°C. Particles smaller than 30 kDa were able to pass the membrane into the filtrate collector and thrown away, while all particles above the 30 kDa, like the isolated protein, retained in the sample container.

The sample container was filled with approximately 15 mL protein solution and then centrifuged at 2500 rpm at 4 °C for 20 min. After centrifugation the filtrate was discarded and new protein solution was added and again centrifuged until having reached the desired volume.

The next step was desalting with PD-10 column. The column was equilibrated with 25 mL of buffer A. 2.5 mL of the sample were loaded on to the column. To elute the protein 3.5 mL of buffer A were loaded on to the column and the coloured sample, which contained MagKatG1, was collected and then applied to a hydroxyapatite column.

Material:
Buffer A: 5 mM phosphate buffer pH 7.5

Equipment:
Amicon Centriprep 30
PD-10 column (GE healthcare)
Centrifuge: Sorval Instruments, RC5 or RC6
Rotor: SLA-1500

5.4. Chromatography with hydroxyapatite (HA)

A second chromatography step guarantees a higher purification and the separation of 2 forms of the enzyme: the high spin form (high catalase activity) and the low spin form. Hydroxyapatite is a mineral form of calcium apatite with the formula $Ca_5(PO_4)_3(OH)$. The interactions are not trivial due to nonspecific interactions between positively charged calcium ions and negatively charged phosphate ions on the gel vs. negatively charged carboxyl groups and positively charged amino groups from the protein.

5 mL of obtained protein solution were loaded on to the HA column (equilibration with running buffer A). Three different elution steps are performed with increasing phosphate concentration and pH-value (running buffers A, B and C) which led to 3 different protein pools. Pool A and B contained the high-spin form of MagKatG1 and pool C contained the low-spin form of the enzyme.
The flow rate was 1.5 mL min^{-1} and fractions of 1.5 mL were taken. Concentration of the pools was performed as described above.

Material:

Running buffer A: 5 mM phosphate buffer pH 7.5
Running buffer B: 50 mM phosphate buffer pH 7.7
Running buffer C: 250 mM phosphate buffer pH 8.0

Equipment:

Gel: Hydroxyapatite (Sigma)
Peristaltic Pump
Fraction collector
Ultrasonic bath (Bandelin Sonorex Super RK 510H)

5.5. Electrophoresis – SDS-PAGE

Many Biomolecules carrying a charge can move in an electric field. The mobility of the ions depends on charge, size and shape of the molecules. These differences are the basis of electrophoresis. The electrophoretic separation occurs in inert, homogenous gels like polyacrylamide gel (PAGE).
Sodium dodecyl sulphate (SDS) is an anionic detergent, which binds dominantly to proteins causing denaturation thereby conferring a net negative charge to the protein. The proteins then have a mobility which is inversely proportional to their size.

SDS-PAGE was used to analyse the MagKatG1 samples and determine the purity of protein samples.

After MCAC and HA chromatography, the MagKatG1 samples were mixed with NuPAGE LDS sample buffer (4x), 2-Mercaptoethanol and RO-H_2O and incubated at 70 °C for 10 min. Electrophoresis was performed at constant 200 V for about 75 min. Afterwards the gel was rinsed with RO-H_2O and prepared for staining or stored at 4 °C.

Material:

NuPAGE Novex Bis-Tris mini Gel gradient 4-12% (1 mm) or without gradient 12%

NuPAGE LDS sample buffer (4x)

NuPAGE MOPS SDS running buffer (for „mid-size“-proteins)

2-Mercaptoethanol (conc.)

Equipment:

Bio-Rad Mini-Protean system

5.6. Detection

There are two common ways to visualize the protein bands: staining with Coomassie Brilliant Blue or the detection with antibodies and visualisation due to an alkaline phosphatase.

5.6.1. Detection with Coomassie Brilliant Blue

The gel was agitated with staining solution for approximately 30 min until the bands were clearly visible. Then the gel was treated with destaining solution for 1 to 3 hours until the background was colourless. The destaining solution had to be changed several times. After the destaining step the gel was stored in RO-H_2O at 4°C.

Material:

Solution for staining:

0.1% ($^{w}/_{v}$) Coomassie Brillinant Blue R-250

40% ($^{v}/_{v}$) Methanol

10% ($^{v}/_{v}$) glacial acetic acid

50% ($^{v}/_{v}$) RO-H_2O

Solution for Destaining:

40% ($^{v}/_{v}$) Methanol

10% ($^{v}/_{v}$) glacial acecitc acid

50% ($^{v}/_{v}$) RO-H_2O

5.6.2. Immunodetection

The captured gel from electrophoresis was equilibrated in transfer buffer a few minutes and then transferred to the Novex Semi Dry Blotter as follows:

- Ensure at every single step of the procedure that there are no air bubbles!
- Humidify 2 pieces of filter paper (thickness of 2.5 mm) with transfer buffer and transfer them to the wet anode of the device.
- Place the pre-soaked blotting membrane on top of the filter paper.
- Transfer the gel onto the blotting membrane. Do not move the gel after it has been placed (can result in protein smearing on the membrane).
- Place 2 pieces of wet filter paper (thickness of 2.5 mm) on top of the gel.
- Close the device and run it at 20 V for about 45 min.

After blotting following steps were performed:

- Incubate the membrane in blocking buffer at 4°C over night.
- Treat the membrane with primary antibody solution (diluted 1:1000 in binding buffer) at room temperature.
- Perform 2 washing steps with binding buffer. Each step: 10 min.
- Incubate the membrane in the second antibody (diluted 1:15000) for 60 up to 120 min at room temperature.
- Perform 4 washing steps with binding buffer. Each step: 10 min.
- Rinse well the membrane with RO-H_2O.
- Incubate in AP-buffer for setting the correct pH (2 times for 5 min).
- Cover the membrane with BCIP/NBT-solution and incubate at room temperature for up to 30 min in darkness until dark purple bands are observable.

<u>Material:</u>

Transfer Buffer (2x):

25 mL NuPAGE Transfer Buffer (20x)
25 mL Methanol
450 mL RO-H_2O

PBS (phosphate-buffered saline):

8.0 g NaCl

0.2 g KCl

2.73 g $Na_2HPO_4*7H_2O$

0.24 g KH_2PO_4

Add 900 mL RO-H_2O, set pH to 7.4 and fill up to 1000 mL with RO-H_2O.

Blocking / Binding Buffer:

2% ($^{w}/_{v}$) BSA in PBS

Antibody 1: Anti-catalase-peroxidase from *Neurospora crassa*

Antibody 2: Sigma Anti-Rabbit IgG, AP Conjugate (Cat. No.: A3857)

Alkaline phosphatase buffer:

100 mM Tris-HCl (pH 9.0)

150 mM NaCl

1 mM $MgCl_2$

BCIP/NBT-solution:

NBT (nitro blue tetrazolium) formulation: NBT (50 mg/mL) in 70% dimethylformamide

BCIP (5-bromo-4-chloro-indolyl-phosphate) Formulation: BCIP (50 mg/mL) in 100% dimethylformamide

Composition of Color Development Substrate (Cat. No.: S3771):

Add 33 µL NBT and 16.5 µL BCIP to 5 mL of alkaline phosphatase buffer. Add the NBT first, mix well, then add the BCIP and mix again.

<u>Equipment:</u>

Invitrogen Novex Semi Dry blotter

Membrane: Amersham Hybond ECL Nitrocellulose Membrane

Blotting filter paper

5.7. Steady-state kinetics

5.7.1. Catalase activity

Catalase activity was determined spectrophotometrically by measuring the consumption of H_2O_2 at 240 nm (Assay concentrations: Volume: 3 mL, 100 mM phosphate pH 6.0, 10 mM H_2O_2). The reaction of MagKatG1 and hydrogen peroxide leads to a decrease in relative absorbance, and the linear range of the time trace was used for the determination of the catalase-activity.

For calculation of the hydrogen peroxide decrease, the Lambert Beer law $\Delta E = c \times \varepsilon \times d$ was used, where ε is the molar extinction coefficient for H_2O_2 at 240 nm (ε_{240} of 42.9 M^{-1} cm^{-1}), d is the distance (cm^{-1}) the light travels through the substance and ΔE is the difference in relative absorbance at 240 nm.

One Unit of catalase is defined as the amount of enzyme that decomposes 1 µmol of H_2O_2 per second at pH 6.0 and 25°C.

Materials:

Hydrogen peroxide (30% H_2O_2 Sigma)

Equipment:

Hitachi Photometer U-3000

3 mL quartz cuvette

Magnetic stirrer

Assay:

100 mM phosphate buffer pH 6.0

10 mM H_2O_2

20 nM MagKatG1

5.7.2. Peroxidase activity

Peroxidase activity was determined spectrophotometrically with a solution containing 4 mM guaiacol and 1 mM peroxyacetic acid in 36 mM phosphate buffer pH 5.5. The reaction was

started by adding ~ 0.12 mg of MagKatG1. This reaction leads to an increase of relative absorbance, and a linear range of the time trace was used for calculation.
For calculation of the decomposed concentration of guaiacol, the Lambert Beer law $\Delta E = c \times \varepsilon \times d$ was used, where ε is the molar extinction coefficient for guaiacol at 470 nm (ε_{470} of 26600 $M^{-1} \times cm^{-1}$), d is the distance (cm^{-1}) the light travels through the substance and ΔE is the difference in relative absorbance at 470 nm.
One Unit of peroxidase is defined as the amount of enzyme that decomposes 1 µmol of guaiacol per second at pH 5.5 and 25°C.

Materials:
Peroxyacetic acid (5.79 M, Sigma)
Guaiacol

Equipment:
Hitachi Photometer U-3000
3 mL quartz cuvette
Magnetic stirrer

Assay:
36 mM phosphate buffer pH 5.5
4 mM guaiacol
1 mM peroxyacetic acid
1.4 µM MagKatG1

5.8. Pre-steady-state kinetics

Pre-steady-state kinetics includes fast reactions which can be measured with a technique called stopped-flow spectroscopy. It is used for studying fast reactions over timescales of about 1 ms up to 100's seconds. In general, 2 reagents are rapidly mixed and then stopped in an observation cell (optical cell). The reaction is proceeding within this cell and detected by either a photomultiplier or a diode array detector. Detection by a diode array will give a wide range of wavelength; the change in spectrum over time can be monitored. Detection using a photomultiplier will result in a time trace which shows the absorbance change of a single wavelength over time.

Figure 8 shows the main components of a stopped-flow apparatus that are a mixing device, observation cell, a stop syringe, a detection system and a recording system capable of responding very rapidly.

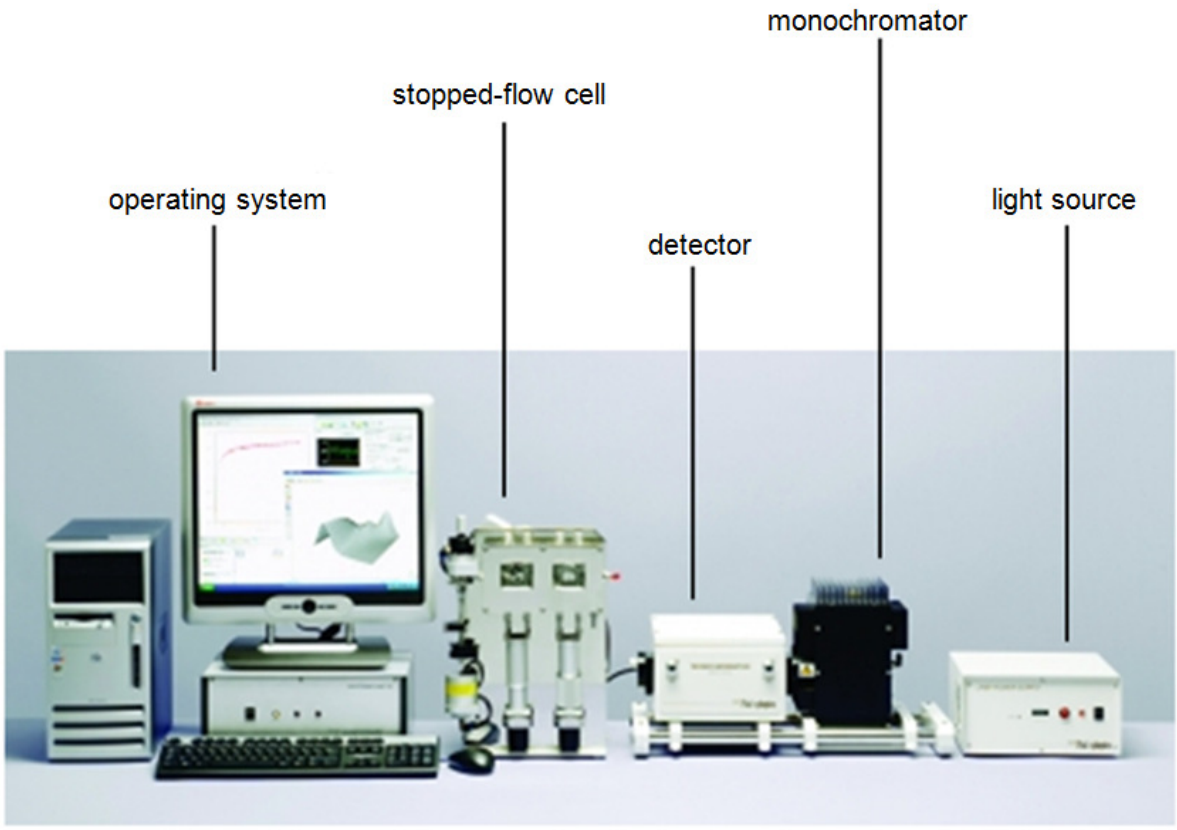

Figure 8: *Components of the SX20 Stopped-Flow Sprectrometer from Applied Photophysics: light source, stopped-flow cell, monochromator, detector and an operating system.*

The advantages of the stopped-flow technique are measuring fast reactions detection of short lived intermediates.

There are two common modes to use stopped-flow spectroscopy: single-mixing mode and sequential-mixing mode. It is important to mention that it has to be assured that only the desired solutions reach the observation cell and no other impurities stay there.

1. Single-mixing mode (see Figure 9): This mode is working with 2 syringes which are filled with an enzyme and a proper substrate, respectively, and mixed directly in the observation cell where the reaction is proceeding. The reagents are contained in two drive syringes (C and F). A drive ram pushes the syringes pistons such that the reagents are pushed through flow tubing to a mixer and then to the observation cell.

This process pushes the 'old' contents of the cell towards the stop-syringe. The flow fills the stop-syringe, until the piston hits the trigger-switch; this action simultaneously stops the flow and starts the data acquisition.

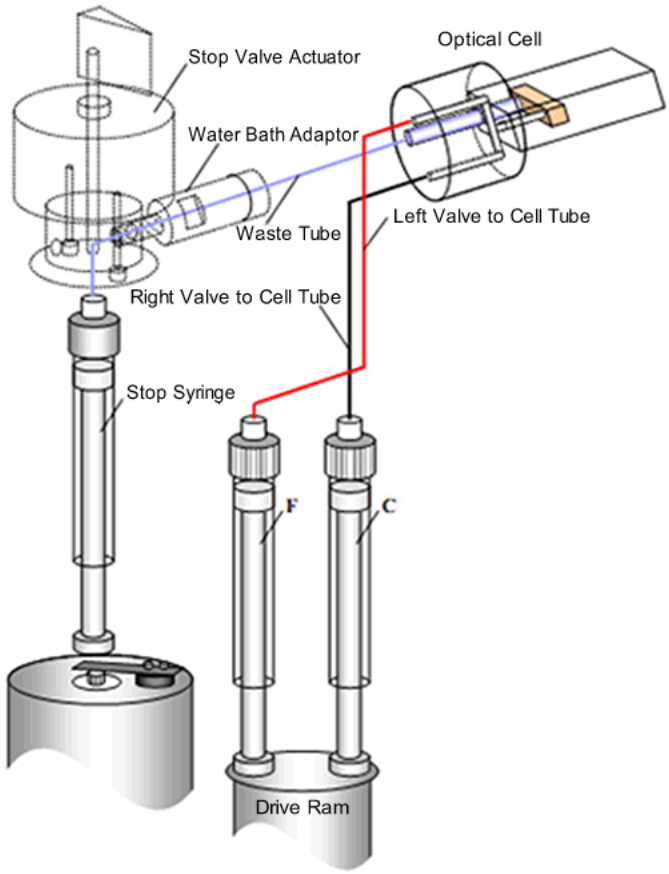

Figure 9: *Components of a stopped-flow apparatus for single-mixing mode: a drive ram, 2 syringes (F, C) for enzyme and substrate, an optical cell and a stop syringe connected to the stop valve actuator.*

2. Sequential-mixing mode (see Figure 10): This setup is commonly used to investigate the reaction between a short-lived reaction intermediate and a second substrate. Additional to the single-mixing mode 2 syringes more and a 4-way coupler is involved in the process. The first step is to create the intermediate within the 4-way coupler being held in an ageing loop, and then the intermediate and the second substrate are mixed within the observation cell where the reaction is monitored. The time of the intermediate staying in the ageing loop is called delay time and can be set electronically.

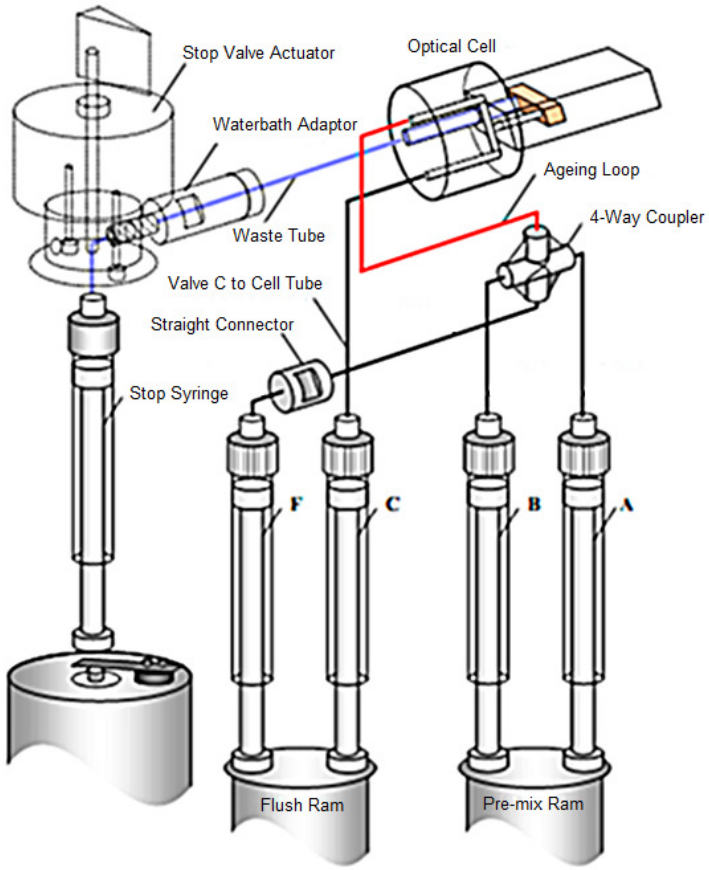

Figure 10: *Components of a stopped-flow apparatus for sequential-mixing mode. In general, the components are the same as for single-mixing mode (see* **Figure 9***). Additionally, another 2 syringes (B, A) are used which contain the enzyme and substrate, respectively and are controlled by the pre-mix ram. In this case syringe C contains the substrate for the intermediate and syringe F serves as a push for the intermediate into the optical cell.*

5.8.1. Compound I-formation

The aim of the measuremets with stopped-flow spectroscopy was to monitor the conversion of ferric enzyme to Compound I with the following substrates: hydrogen peroxide (H_2O_2), peroxyacetic acid (PAA) and hypochlorite (OCl^-) and the determination of their corresponding rate constants k_1.

Due to the fast reaction of ferric MagKatG1 and Compound I with H_2O_2 it is not that easy to determine rate constants for Compound I formation and reduction. The rate constants were determined with peroxyacetic acid and hypochlorite and monitoring of the spectral changes

was able. Rate constants for the formation of Compound I (with PAA and OCl^-) and the back reaction (from Compound I to ferric enzyme with H_2O_2) were determined.

To obtain the rates mentioned above the enzyme (final concentration: 2 µM) diluted in an appropriate buffer (final concentration: 100 mM phosphate buffer pH 7.0) was mixed with PAA (final concentrations ranged from 1 mM to 5 mM) or OCl^- (final concentrations ranged from 30 µM to 100 µM) and then the proceeding reaction was recorded. Measurements started at the lowest concentration level and ended at the highest concentration level to ensure the correct dilutions.

Before and after measurement the syringes, loops and observation cell were washed with RO-H_2O to ensure that no impurities were left. Before the measurement a certain volume of the substrate concentration that had to be measured was pushed through the system to guarantee that the actual substrate concentration was in front of the mixer.

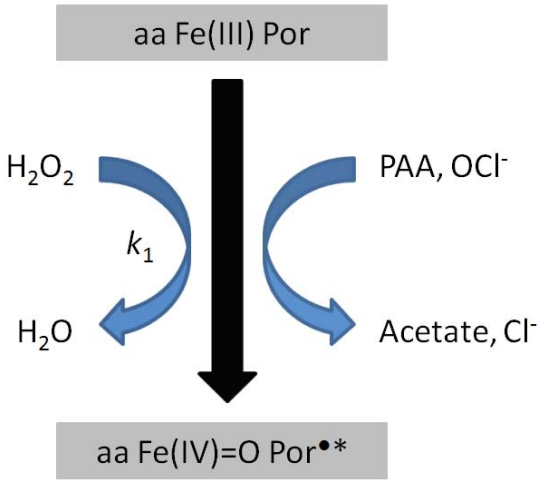

Figure 11: *Formation of Compound I with either the natural substrate (hydrogen peroxide) or with other substrates (peroxyacetic acid, hypochlorite).*

Monochromatic detection of the reaction and fitting (single exponential evaluation) of the time traces leads to different k_{obs} [s^{-1}] at different substrate concentrations. Plotting of k_{obs} versus the corresponding substrate concentration will give a linear dependency with a slope of k_1.

In general, formation of Compound I and formation of ferric enzyme from Compound I (see 5.8.2) behave like second order reactions (A + B → C + D, bimolecular reaction). This can be simplified by increasing the concentration of one reactant. The concentration of the increased reactant must be at least 10 times higher than the other reactant to assume the increased

reaction partner as constant during the reaction. The reaction now behaves as a first order reaction and it is called a pseudo-first order reaction. The velocity $v = k$ [A] [B] becomes $v = k' \times$ [A] as k' includes [B] and k' is the pseudo-first order rate constant.

5.8.2. Formation of ferric enzyme from Compound I

After measuring the observed rate constants (k_{obs}) and calculation of bimolecular rate constant k_1 for the reaction of ferric enzyme to Compound I, the reaction from Compound I to ferric enzyme was performed. The sequential-mixing mode was used to determinate the observed rate constants k_{obs} for H_2O_2 and the corresponding bimolecular rate constant k_5 were calculated.

The reaction of Compound I with H_2O_2 is given as Reaction (5) in Figure 6:

aa Fe(IV)=O $Por^{\bullet+}$ + H_2O_2 → aa Fe(III) Por + H_2O + O_2.

This reaction can only be detected when cyanide is added. The trick is that every single generated ferric enzyme binds irreversibly a CN^- ion and is leaving the catalatic cycle until all catalase-peroxidase molecules exist as enzyme-cyanide-complexes (as low-spin (LS) complex). Otherwise the enzyme would cycle and it wouldn't be possible to detect the conversion from Compound I to the ferric state. In this case, trapping the ferric enzyme with CN^-, the actual rate constants for Compound I reduction can be measured.

The transformed reaction with H_2O_2/CN^- is given as:

aa Fe(IV)=O $Por^{\bullet+}$ + H_2O_2 + CN^- → aa Fe(III) Por-CN^- + H_2O + O_2.

Final concentrations for this reaction step were as follows: 2 µM MagKatG1, 100 µM PAA (delay time: 8000 ms), 50 µM OCl^- (100 ms or 1000 ms resulting in two different forms of Compound I), 1 mM CN^- and 250 to 2000 µM of H_2O_2.

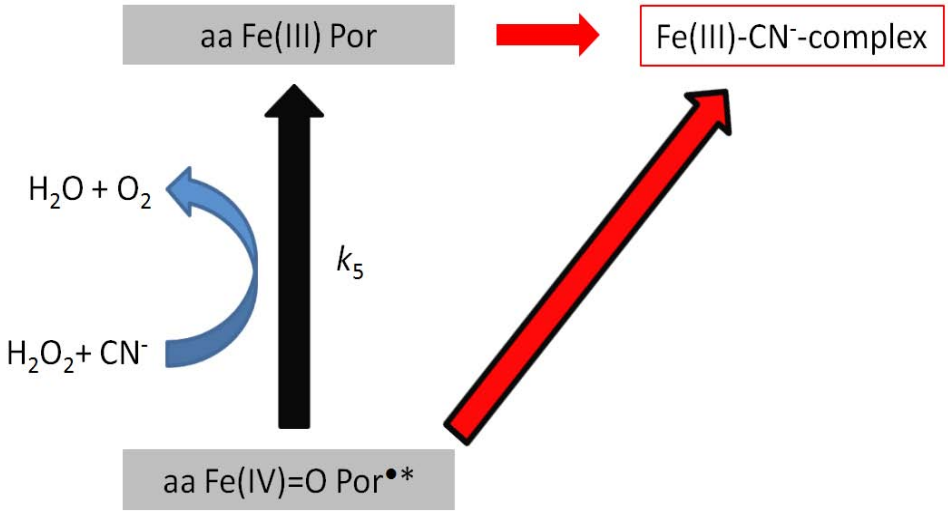

Figure 12: *Formation of ferric enzyme and furthermore Fe(III)-CN$^-$-complex with a mixture of H_2O_2 and cynide. Compound I was formed either with peroxyacetic acid or hypochlorite. The black and red arrows symbolize the 2 steps of the reaction. The red arrow with black edge shows the visible conversion of Compound I to the ferric enzyme-cynide-complex.*

Monochromatic detection of the reaction and fitting (single exponential evaluation) of the time traces leads to different k_{obs} [s^{-1}] for different substrate concentration. Plotting of k_{obs} and versus the corresponding substrate concentration will give a linear dependency leading to a slope representing k_5.

Materials:

Hydrogen peroxide 30% solution

OCl^--solution from Sigma

PAA

CN^-

The HOCl stock solutions were prepared in 5 mM NaOH and stored in the dark. The HOCl concentration was determined spectrophotometrically shortly before the experiments (ε_{295} is 350 M^{-1} cm^{-1}).

Equipment:

Sequential stopped-flow apparatus (Model SX-18MV) from Applied Photophysics

6. Results and Discussion

6.1. Spectrum of MagKatG1

The first purification step was performed with metal chelate affinity chromatography (MCAC). Figure 13 represents the spectrum of ferric MagKatG1 from pool B. The total amount of protein can be calculated via the peak with an absorbance maximum at 280 nm and the amount of MagKatG1 is given by the peak at 407 nm (absorbance maximum, Soret peak). The purity number (Reinheitszahl) of this sample is 0.68. The extinction coefficient ε for MagKatG1 is 110650 $M^{-1}cm^{-1}$ and the Lambert Beer law $E = c \times \varepsilon \times d$ leads to a concentration of this protein fraction of 34.5 µM. In the visible range two more peaks can be seen at about 540 nm and 645 nm.

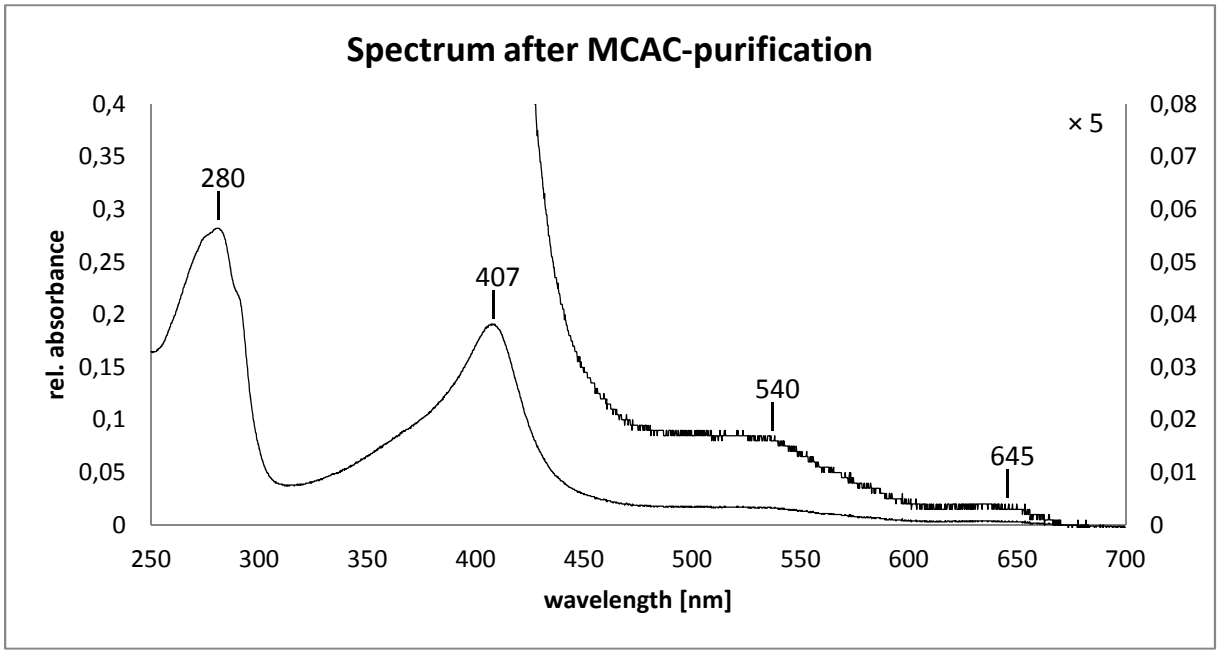

Figure 13: *Spectrum of ferric MagKatG1 after purification with metal chelate affinity chromatography. This spectrum shows one fraction (diluted 1:20) of the second peak that eluted.*

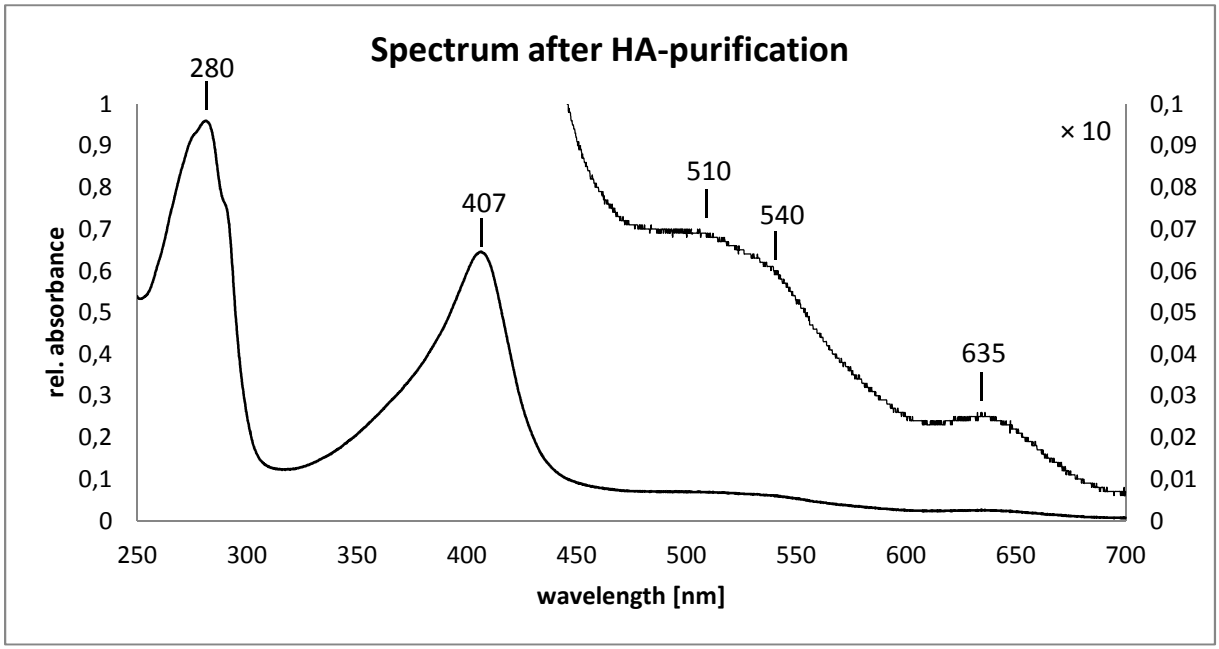

Figure 14: *This spectrum was taken after the 2nd purification step (hydroxyapatite chromatography, fraction with 50 mM phoshpate buffer, pH 7.7) as the high spin (HS, can be seen here) form was separated from the low spin (LS) form.*

Figure 14 shows the spectrum of ferric MagKatG1 after purification with hydroxyapatite chromatography. The total amount of protein can be calculated with the absorbance at 280 nm or with the absorbance at 407 nm (Soret peak) which shows only the amount of active MagKatG1. The purity number i.e. A_{408}/A_{280nm}, is 0.67 and varied over the range 0.63–0.67, which is comparable with values for heterologously expressed prokaryotic KatGs and indicates 100% heme occupancy [C. Jakopitsch, 1999].

Ferric MagKatG1 exhibits the typical bands of a heme *b*-containing peroxidase in the visible and near-UV region with a Soret band at 407 nm, Q-bands at 510 nm and 540 nm and a CT1 band (porphyrin-to-metal charge-transfer band) at 635 nm. This compares with the corresponding SynKatG absorption maxima at 406 nm (Soret), 502 and 542 nm (Q-bands) and 637 nm (CT1) which have been demonstrated to be representative of a five-coordinate high-spin heme coexisting with a small portion of six-coordinate HS heme and a six-coordinate LS haem, as has been demonstrated by resonance Raman spectroscopy of the prokaryotic protein [C. Jakopitsch, 2007]

6.2. Detection with Coomassie Brilliant Blue and Immunodetection

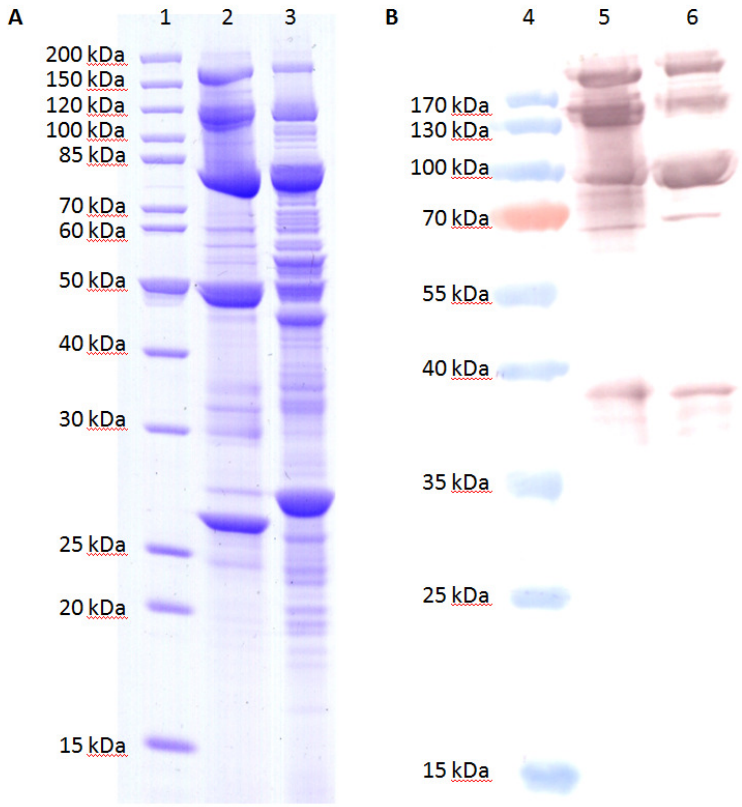

Figure 15: *SDS-electrophoresis with Coomassie Brilliant Blue (A) and immunodetection (B) and 2 different protein ladders were taken: unstained (A) and prestained (B). Lane 1 and 4 show the protein ladders. Lane 2 and 5 are the pooled fractions of high-spin MagKatG1 and lane 3 and 6 show pooled fractions of low-spin MagKatG1.*

Staining of SDS-electrophoresis gels was done either with Coomassie Brilliant Blue staining (see Figure 15 – A) or immunodetection and consecutive staining (see Figure 15 – B). Line 1 shows an unstained protein ladder with following protein sizes (in kDa) starting from the top: 200, 150, 120, 100, 85, 70, 60, 50, 40, 30, 25, 20 and 15. Line 4 shows a pre-stained protein ladder with following protein sizes (in kDa) starting from the top: 170, 130, 100, 70, 55, 40, 35, 25 and 15. Lane 2 gives the migration of high-spin MagKatG1 (pooled fractions which eluted at 5 mM phosphate buffer, pH 7.5, and 50 mM phosphate buffer, pH 7.7). Lane 3 shows the migration of low-spin MagKatG1 (pooled fraction which eluted at 250 mM phosphate buffer pH 8.0). Evaluation was done as plotting the logarithmic molar mass (kDa) versus the length of migration of the protein ladder.

Protein size was calculated with the linear regression model and the formula $y = -0.011x + 2.1031$ (see Figure 16) led to a calculated protein size of 82.4 kDa.

There are 5 prominent bands in lane 2 at about 170, 109, 96, 82, 55 and 26 kDa. The 82 kDa band represents the monomer of MagKatG1 that is confirmed by the Western blot shown in lane 4. The calculated molar mass of 82.4 kDa corresponds to theoretical molar mass of a monomer with one heme *b* and a His_6-tag (83.2 kDa). The band at 170 kDa suggested the presence of a covalently linked dimeric form of MagKatG1. The other bands at 55 and 26 kDa gave positive signals suggesting proteolytic degradation of MagKatG1. By MS analysis, it was shown that the bands at 51 and 31 kDa gave positive signals due to proteolytic degradation of MagKatG1. [M. Zamocky, 2009b]

Lane 3 shows more bands. These bands are at about 170, 112, 82, 59, 54, 49 and 27 kDa which are similar compared to lane 2 but it seems that there are more proteolyic degradation products or impurities within. The monomer of MagKatG1 is again at about 82 kDa which is confirmed also in lane 6.

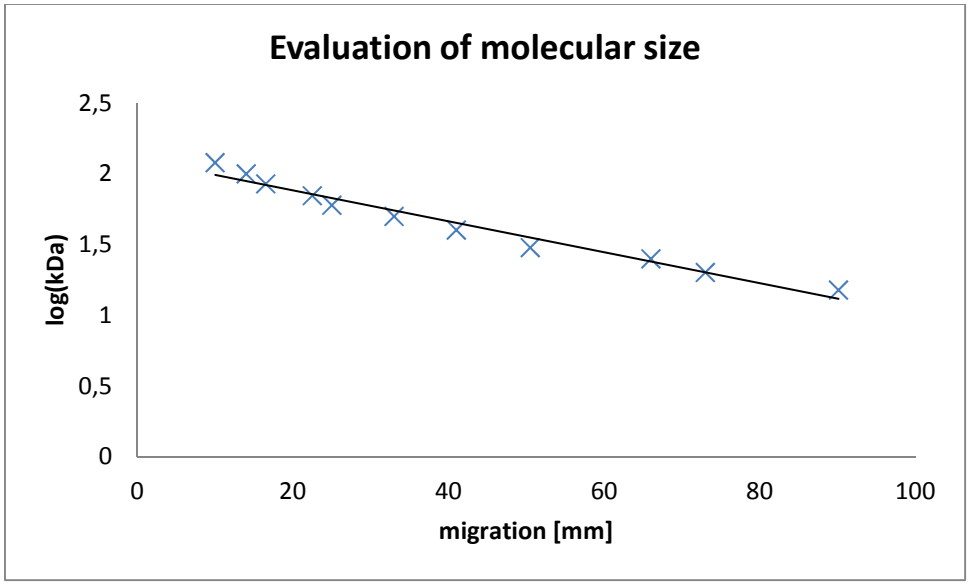

Figure 16: *Plot of protein ladder (logarithmic values of kDa) versus the length of migration in mm for evaluation of the electrophoresis (staining with Coomassie Blue Brilliant – see* Figure 15 *– A)*

6.3. Steady-state kinetics

6.3.1. Reaction of ferric MagKatG1 with H_2O_2

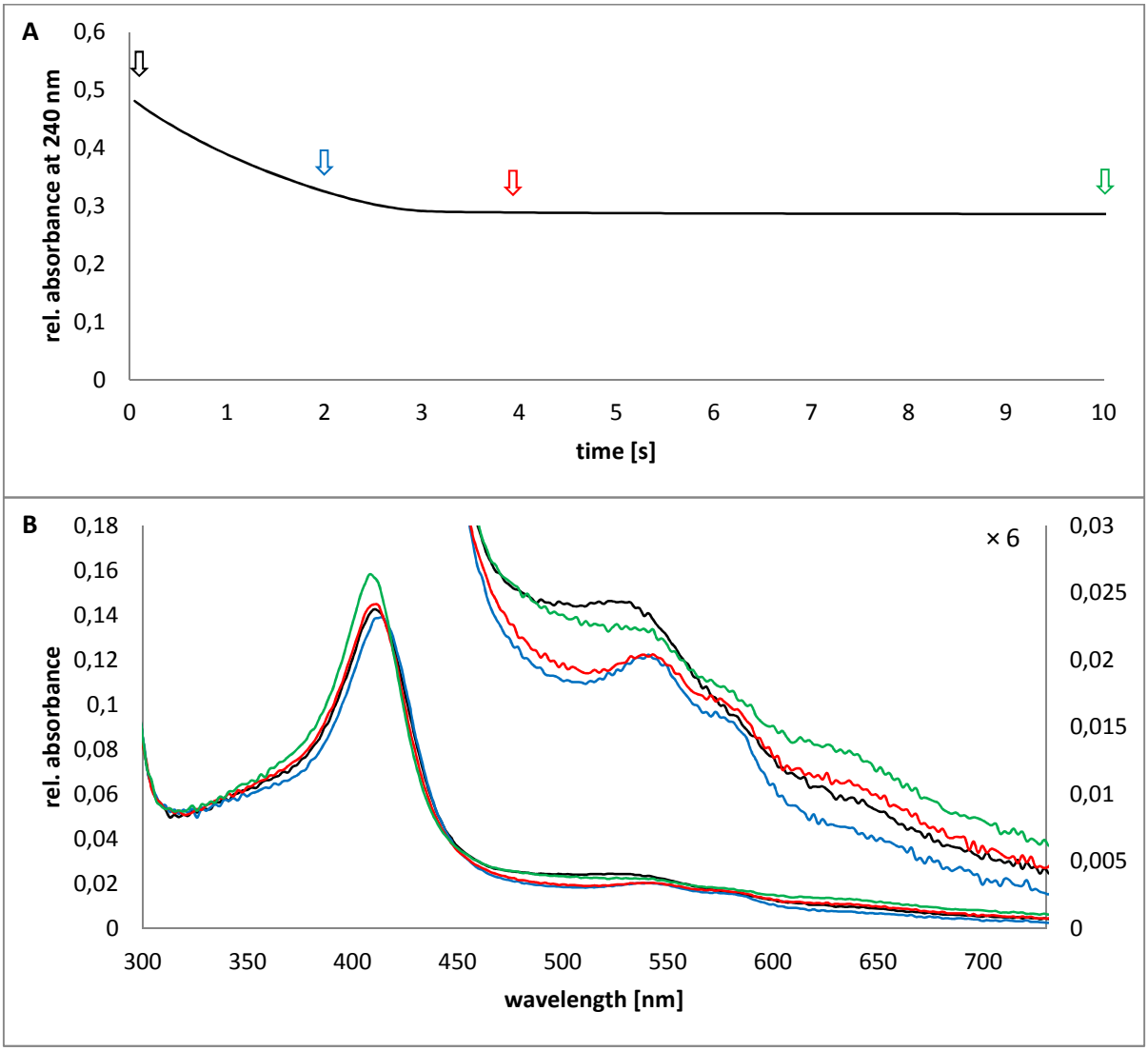

Figure 17: *Consumption of 5 mM H_2O_2 by 1.4 µM MagKatG1. The coloured arrows (**A**) indicate the time point when the corresponding spectrum was recorded (**B**).*

The reaction of ferric enzyme with three different concentrations of hydrogen peroxide (5, 10 and 20 mM H_2O_2, see Figure 17, 18 and 19, respectively) has been investigated. The consumption of H_2O_2 and selected spectra at specific time points for each reaction were determined – at the beginning of the reaction, during hydrogen peroxide consumption, after

H_2O_2-consumption and at the very end of the reaction (shown in Figure 17, Figure 18 and Figure 19).

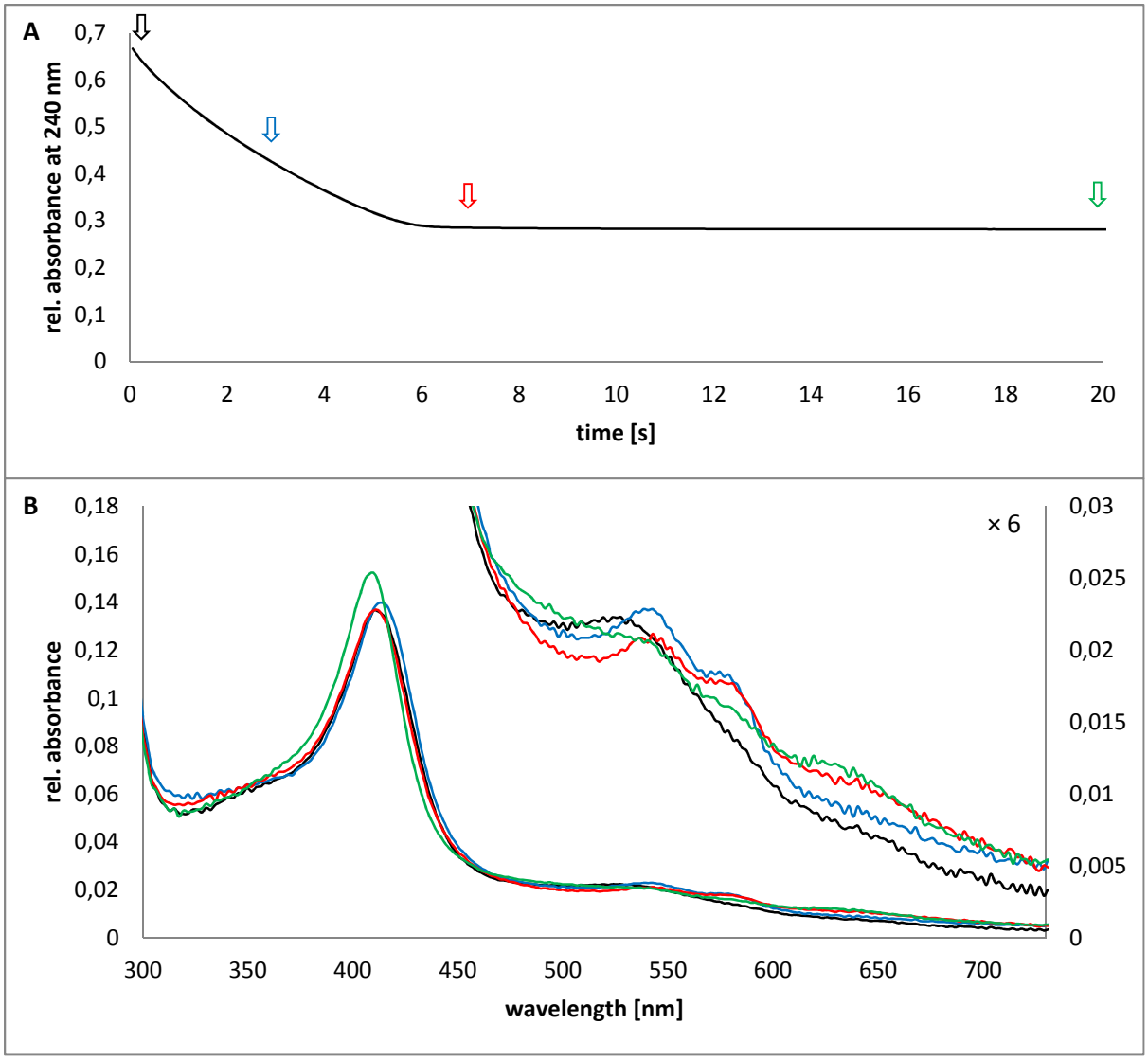

Figure 18: *Consumption of 10 mM H_2O_2 by 1.4 µM MagKatG1. The coloured arrows (**A**) indicate the time point when the corresponding spectrum was recorded (**B**).*

Black spectra were recorded after 1.3 ms after the reaction was started and showed under all three conditions the ferric enzyme with the Soret maximum 409 nm, and an absorbance band at 520 nm.

Blue spectra indicated the middle of the reaction where approximately half of the hydrogen peroxide was consumed. These spectra showed a hypochromic and red shifted Soret maximum (414 nm), a hyperchromic shift in the Q-band region (540 and 580 nm), and disappearance of the high-spin CT band at 635 nm. Generally, increasing amounts of H_2O_2 caused an increased more pronounced red shift of the Soret band within 1.3 ms of mixing,

and the reaction intermediate was evident only until all of the hydrogen peroxide was consumed.

Red spectra were recorded when all the hydrogen peroxide was consumed and a mixture of oxidized and ferric enzyme can be observed (end of reaction and transition into ferric enzyme).

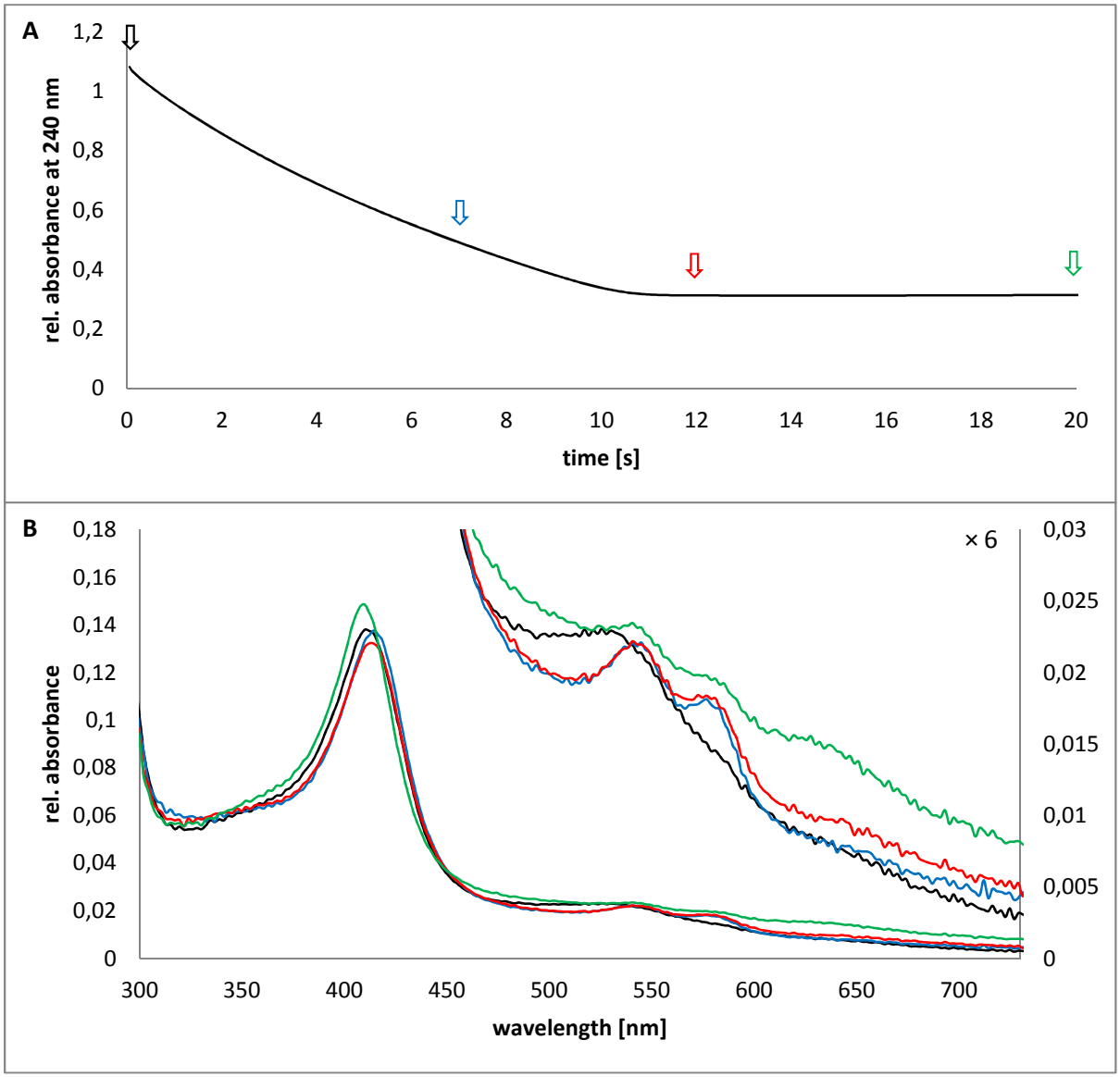

Figure 19: *Consumption of 20 mM H_2O_2 by 1.4 µM MagKatG1. The coloured arrows (**A**) indicate the time point when the corresponding spectrum was recorded (**B**).*

Finally the green spectra (recorded after 10, 20 and 20 s for 5, 10 and 20 mM H_2O_2-concentration, respectively) are formed after a distinct time when all hydrogen peroxide was exhausted. At this time the enzyme shows the highest absorbance at 408 nm with three

distinct peaks at 540, 580 and 640 nm. This state represents the end of the reaction and concomitantly reforming of the ferric state of the enzyme.

6.3.2. Catalase-activity

Catalase-activity was measured with H_2O_2 following the decrease in relative absorbance at 240 nm (Figure 20).

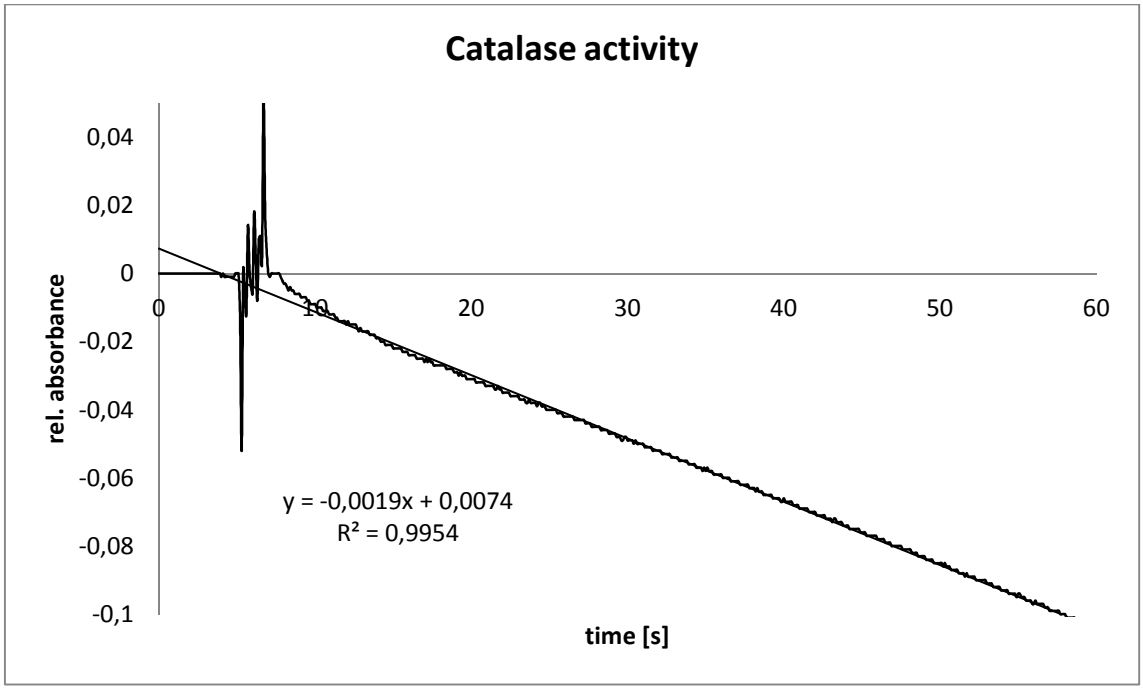

Figure 20: *Decrease in relative absorbance at 240 nm of H_2O_2. The range between 10 and 25 s is used for calculation of catalase activity. 10 µL MagKatG1 (≙ 4.9 µg) were taken from the fraction described above (fraction of HA-purified enzyme, see 6.1).*

The time trace in the range of 10 to 25 s was fitted with a linear function, which resulted in a ΔE of ~0.031 (according to Figure 20: ΔE of 0.0019 per second). Transforming the Lambert Beer law $E = c \times \varepsilon \times d$ (where ε is 42.9 $M^{-1} \times cm^{-1}$ and d is 1 cm) into $\Delta c = \frac{\Delta E}{\varepsilon \times d}$ resulted in 44.3 µM × s^{-1} (v_0). Using 3 mL of H_2O_2-solution for this assay led to 0.133 Units [µmol × s^{-1}]. 4.9 µg MagKatG1 resulted in 27 Units per 1 mg MagKatG1.

By contrast, catalase activity for *Synechocystis* KatG was determined polarographically using a Clark-type electrode. The catalase activity for wild-type SynKatG is 10 Units per 1 mg, so it is 37 % of the activity of MagKatG1. [C. Jakopitsch, 2001]

6.3.3. Peroxidase-activity

Peroxidase-activity was tested with guaiacol and peroxyacetic acid. The oxidation product of guaiacol absorbs at 470 nm and can be measured with a spectrophotometer (Figure 21). For bifunctional catalase-peroxidase peroxyacetic acid was used to avoid that hydrogen peroxide is consumed by the catalatic reaction.

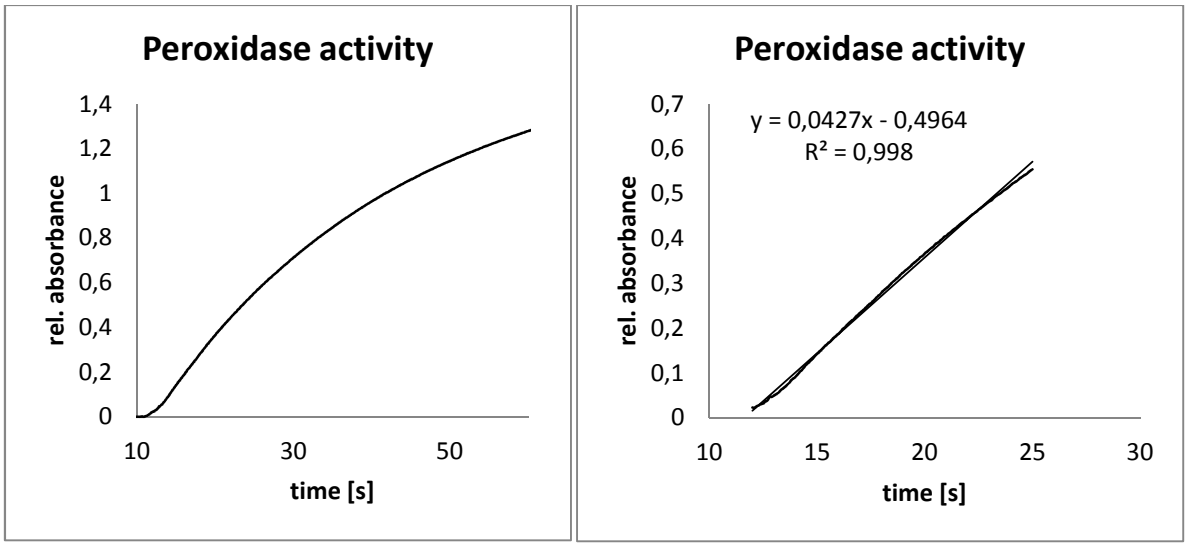

Figure 21: *Increase in relative absorbance at 470 nm measured by oxidizing guaiacol. The range between 12 and 25 s is used for calculation of peroxidase activity.* 100 µL MagKatG1 (≙ 1.44 nmol or 0.12 mg) were taken for this assay.

The time trace in the range of 12 to 25 s was fitted with a linear function, which resulted in a ΔE of 0.532. (according toFigure 21: ΔE of 0.043 per second). Transforming the Lambert Beer law $E = c \times \varepsilon \times d$ (where ε is 26600 $M^{-1} \times cm^{-1}$ and d is 1 cm) into $\Delta c = \frac{\Delta E}{\varepsilon \times d}$ resulted in 1.6 µM × s^{-1}. 1 mL final assay volume led to 0.0016 Units [µmol × s^{-1}]. 0.12 mg MagKatG1 used for the assay resulted in 0.013 Units per 1 mg MagKatG1.

Peroxidase activity for *Synechocystis* KatG was determined spectrophotometrically with H_2O_2 and *o*-diansidine. The peroxidase activity for SynKatG was 0.04 Units/mg, so the activity of MagKatG1 is only 32.5 % compared to the activity of SynKatG. A direct comparison of the peroxidase activity is not possible because SynKatG was measured under different conditions. [C. Jakopitsch, 2001]

6.4. Pre-steady-state kinetics

6.4.1. Compound I-formation with PAA

As has been reported earlier, the catalase activity of wild-type KatGs does not allow one to follow Compound I-formation by addition of hydrogen peroxide. [C. Jakopitsch, 2003a-c] However, upon addition of peroxyacetic acid or hypochlorite a Compound I spectrum can be obtained that is distinguished from the ferric enzyme by a 40-50% hypochromicity, and its formation can be followed as exponential absorbance decrease at the Soret maximum.

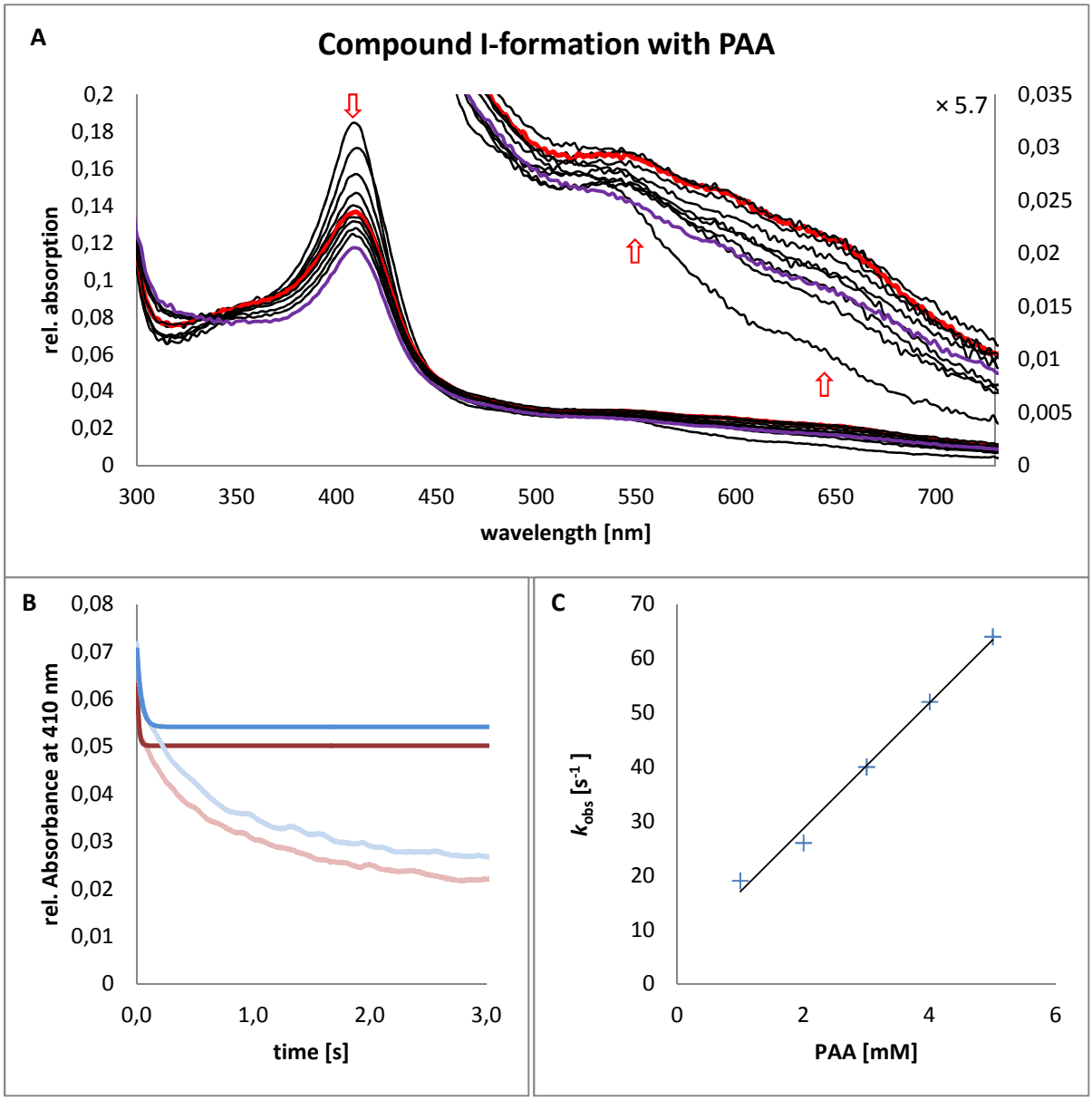

Figure 22: *Compound I-formation with PAA:* ***A*** *shows the formation of Compound I with peroxyacetic acid (spectral transition of 2 µM ferric MagKatG1 upon mixing with 1 mM PAA). The red spectrum represents Compound I after 8 s and the transition to*

*the purple spectrum describes a decay which is not dependent on concentration. Time traces for two measurements (2 and 5 mM PAA-concentration, blue and red, respectively) including the single exponential fits can be seen in **B** and **C** shows the determination of k_1 for Compound I formed with PAA (observed rate constants k_{obs} plotted against PAA-concentration).*

Figure 22**A** shows the spectral transition of 2 µM MagKatG1 with 1mM peroxyacetic acid. The first spectrum with a Soret peak at 408 nm indicates the ferric MagKatG1. Upon addition of peroxyacetic acid a Compound I spectrum can be obtained that is distinguished from the resting state by a hypochromic shift at the Soret maximum. Isosbestic points can be found at 360 and 445 nm. The single spectrum in red was taken after approximately 8 s and represents the spectrum of Compound I which assumed that the ferric enzyme is completely oxidized. At high concentration of peroxyacetic acid Compound I decayed further (spectral transition from red spectrum to the purple Spectrum (40 s after reaction start) most properly due to heme bleaching.

In Figure 22**B**, two time traces at 410 nm can be seen – one for the measurement with 2 mM PAA (light blue) and the other with 5 mM PAA (light red) and the corresponding single exponential fits for the initial reaction (marked in dark blue and dark red, respectively). An increase of peroxyacetic acid led to faster reactions and higher k_{obs} were obtained. The plots of the pseudo-first-order rate constants, k_{obs}, vs. peroxyacetic acid concentration are linear with very small intercepts (Fig. 22B). Concentration dependency was shown for the initial reaction, not for the second part of the reaction. Hence, further decay of the enzyme (transition from red to purple spectrum) is not dependent on PAA-concentration.

The determination of k_1 for the formation of Compound I with PAA can be seen in Figure 22**C** and was performed in a concentration range from 1 to 5 mM PAA. Plotting of k_{obs} against PAA-concentration leads to a linear dependency with a slope of k_1. k_1 for the formation of Compound I with PAA was $1.2 \times 10^4\ M^{-1}\ s^{-1}$.

SynKatG with a k_1 for the formation of Compound I with PAA of $1.3 \times 10^4\ M^{-1}\ s^{-1}$ is similar to MagKatG1 [C. Jakopitsch, 2007].

6.4.2. Compound I-formation with OCl^-

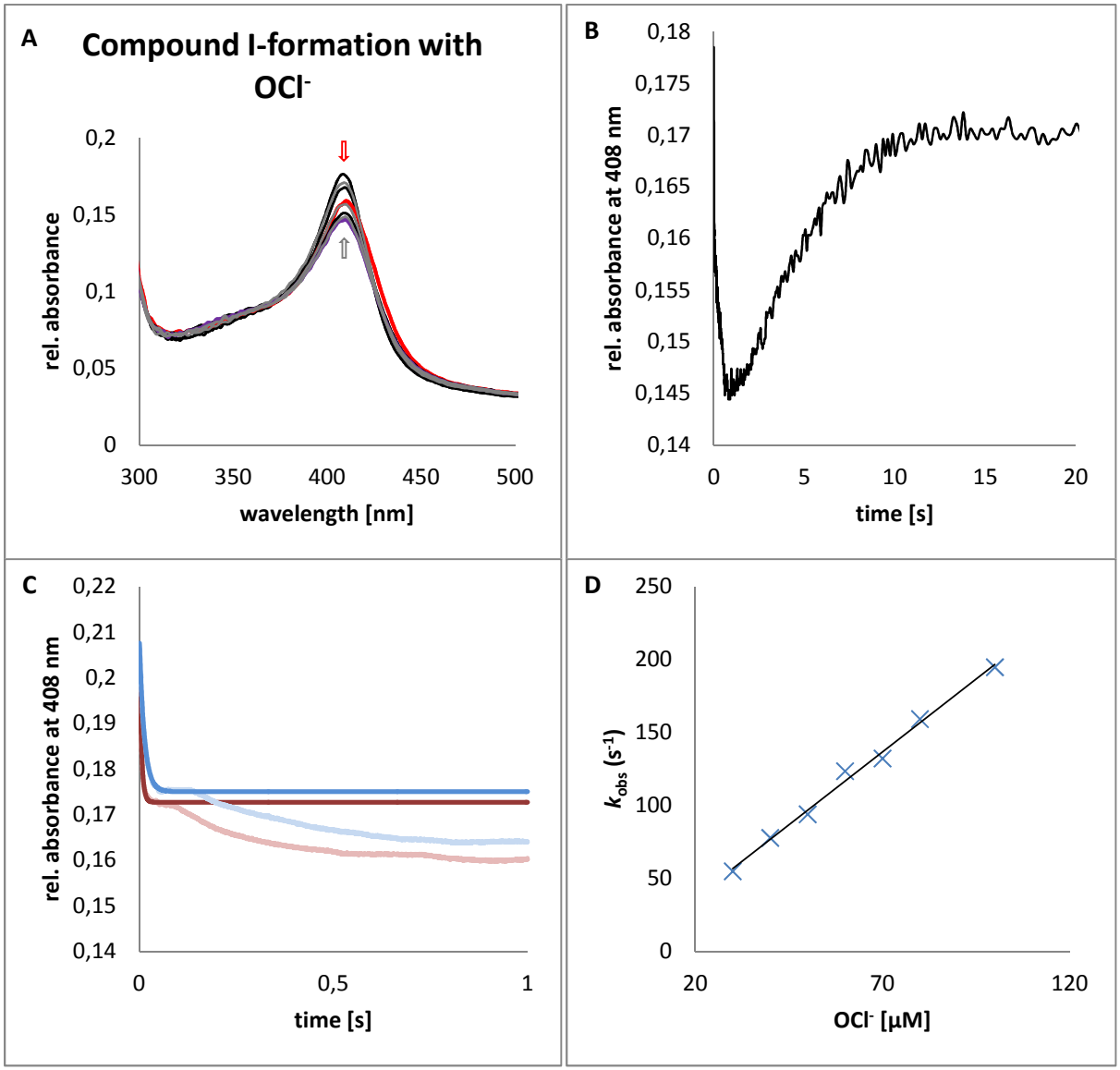

Figure 23: *Compound I-formation with OCl^-: **A** shows the formation of Compound I with hypochlorite (spectral transition of 2 µM ferric MagKatG1 upon mixing with 50 µM OCl^-). The red spectrum represents the 1st intermediate formed (named Intermediate I) and the purple spectrum indicates the 2nd intermediate formed (named Intermediate II). A time trace at 408 nm for 20 s is shown in **B**: spectral transition from ferric enzyme to both Intermediates and back. Time traces for two measurements (40 and 100 µM OCl^- concentration, blue and red, respectively) including the single exponential fits can be seen in **C** and **D** shows the determination of k_1 for the formation of Compound I with OCl^- (observed rate constants k_{obs} plotted against OCl^--concentration).*

Figure 23**A** shows the spectral changes upon addition of hypochlorite of ferric MagKatG1. The first black spectrum with an absorbance maximum at 408 nm (Soret peak) indicates the ferric enzyme. With OCl^- two different reaction intermediates could be found. Within this document, these two intermediates are named Intermediate I and Intermediate II (red and purple spectrum, respectively). Isosbestic points can be found at 370 nm and 418 nm (for the conversion into Intermediate I) and at 380 nm and 470 nm (for the conversion from Intermediate I into Intermediate II). Intermediate I was formed after approximately 100 ms and showed a decrease in relative absorbance and a shift of the Soret peak from 408 to 410 nm. The reaction with hypochlorite proceeded and showed the spectral transition to Intermediate II (after approximately 1000 ms), that can be followed by a further decrease in absorbance at 410 nm and. The peaks at 540 and 640 nm show an increase in rel. absorbance until Intermediate II is formed. Intermediate II is not stable and racts back (spectral changes shown in grey) to the ferric MagKatG1 within approximately 20 s. Compared to the reaction with PAA, oxidized KatG is not trapped and is able to use Cl^- as a substrate to form ferric enzyme again. The spectral change is described by an increase in relative absorbance at the Soret peak and a decrease at 540 and 640 nm. Final concentrations: 2 µM MagKatG1, 50 µM OCl^-, 100 mM phosphate buffer, pH 7.0. Figure 23**B** shows a time trace at 408 nm for 20 s to illustrate the forward and back reaction (ferric enzyme → Intermediate I → Intermediate II → Intermediate I → ferric enzyme). Intermediate II is formed after 1 s and ferric enzyme is formed again after approximately 20 s.

In Figure 23**C** two time traces at 408 nm can be seen – one for the reaction with 40 µM OCl^- (light blue) and the other with 100 µM OCl^- (light red) and the corresponding single exponential fits for the initial reaction (marked in dark blue and dark red, respectively). An increase of hypochlorite led to faster reactions and higher k_{obs} were obtained, but only the transition from ferric enzyme to Intermediate I follows a concentration dependency. The reaction from Intermediate I to II seem to be a conversion which is not dependent on concentration of OCl^-.

The determination of k_1 for the formation of Intermediate I with OCl^- can be seen in Figure 23**D** and was performed in a concentration range from 30 to 100 µM OCl^-. Plotting of k_{obs} against OCl^--concentration leads to a linear dependency with a slope of k_1. k_1 for the formation of Intermediate I with OCl^- is $\underline{2 \times 10^6\ M^{-1}\ s^{-1}}$.

6.4.3. Reaction of Compound I (formed with PAA) and H_2O_2/CN^-

In the following sequential stopped-flow experiments cyanide was present in the reaction mixture in order to suppress cycling of catalase-peroxidase with excess H_2O_2. Principally, ferric KatG has two possibilities to react, namely either with H_2O_2 to Compound I or with cyanide to the corresponding LS complex. Assuming that the unknown rate of compound I formation by H_2O_2 in MagKatG1 is of the same order of magnitude as in other heme peroxidases (k_1~1×10^7 M^{-1} s^{-1}) [J. Vlasits, 2010b], the cyanide concentration had to be at least 10-times higher than that of added H_2O_2. Typically, with MagKatG1 concentrations of H_2O_2 >250 µM and 1 mM NaCN were used.

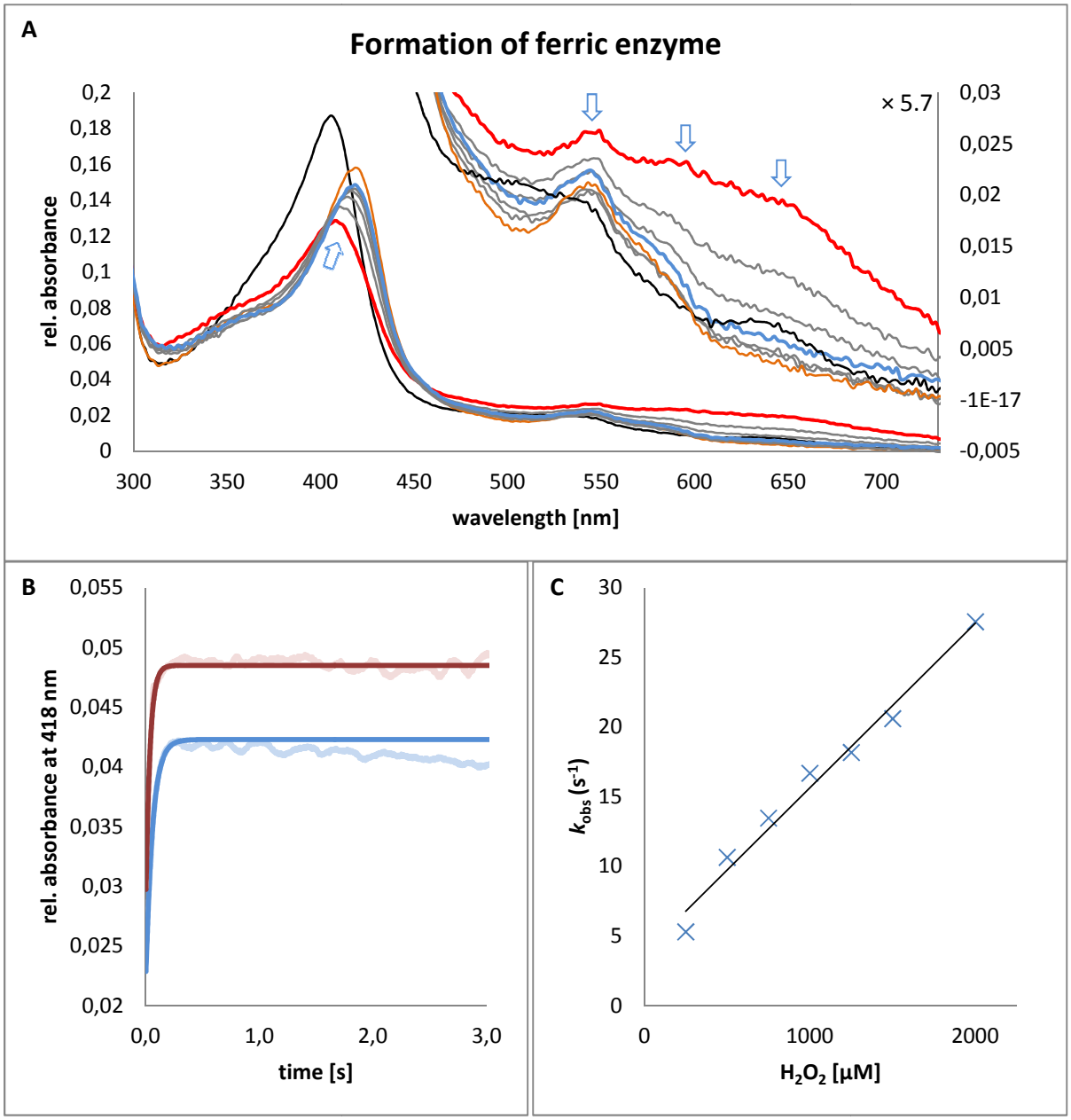

Figure 24: *Reaction of Compound I formed with PAA and H_2O_2/CN^-: **A** shows the spectral transition (shown in grey) of Compound I (1.7 µM ferric enzyme mixed with 100 µM PAA) upon mixing with 1 mM H_2O_2 and 1 mM CN^-. Different states of the enzyme are shown: ferric enzyme (black), Compound I (red), Fe(III)-CN^--complex (from pre-formed Compound I, blue) and Fe(III)-CN^--complex (ferric enzyme mixed with cyanide, orange). Time traces for two measurements (1000 and 2000 µM H_2O_2-concentration, blue and red, respectively) including the single exponential fits can be seen in **B** and **C** shows the determination of k_5 for the formation of ferric enzyme with H_2O_2 (observed rate constants k_{obs} plotted against H_2O_2-concentration).*

Figure 24**A** shows the spectral transition (shown in grey) of Compound I (delay time: 8 s, red spectrum) to the Fe(III)-CN^--complex (blue spectrum). The black spectrum (with a peak

maximum at 406 nm) indicates the ferric enzyme and the orange spectrum (with a peak maximum at 418 nm) shows the Fe(III)-CN^--complex when 1.7 µM ferric enzyme were mixed with 1 mM CN^-. Isosbestic points of the spectral transition of Compound I to the ferric enzyme-cyanide-complex can be found at 400 and 460 nm.
The reaction of Compound I with H_2O_2/CN^- is described by an increase and shift in relative absorbance from 408 to 418 nm. At 540, 590 and 640 nm a decrease in absorbance can be observed during the reaction. The resulting spectrum of this reaction is very similar to the spectrum of the cyanide complex only formed with ferric enzyme. The reaction mechanism and trapping of the ferric enzyme is described in 5.8.2.
Final concentrations: 1.7 µM MagKatG1, 100 µM PAA, 1 mM CN^-, 1 mM H_2O_2, 100 mM phosphate buffer pH 7.0, delay time for Compound I: 8 s.

In Figure 24**B** two time traces at 418 nm can be seen – one for the measurement with 1000 µM H_2O_2 (light blue) and the other with 2000 µM H_2O_2 (light red) and the corresponding single exponential fits for the initial reaction (marked in dark blue and dark red, respectively). An increase of hydrogen peroxide led to faster reactions and higher k_{obs} were obtained.

The determination of k_5 for the formation of ferric enzyme with H_2O_2 can be seen in Figure 24**C** and was performed in a concentration range from 250 to 2000 µM H_2O_2. Plotting of k_{obs} against H_2O_2-concentration leads to a linear dependency resulting in a slope of k_5. k_5 for the formation of ferric enzyme with H_2O_2 is $1.2 \times 10^4\ M^{-1}\ s^{-1}$.

SynKatG with a k_5 for the formation of ferric enzyme from Compound I pre-formed with PAA of $1.2 \times 10^4\ M^{-1}\ s^{-1}$ is the same as MagKatG1 [J. Vlasits, 2010b].

6.4.4. Reaction of Intermediate I (formed with OCl^-) and H_2O_2/CN^-

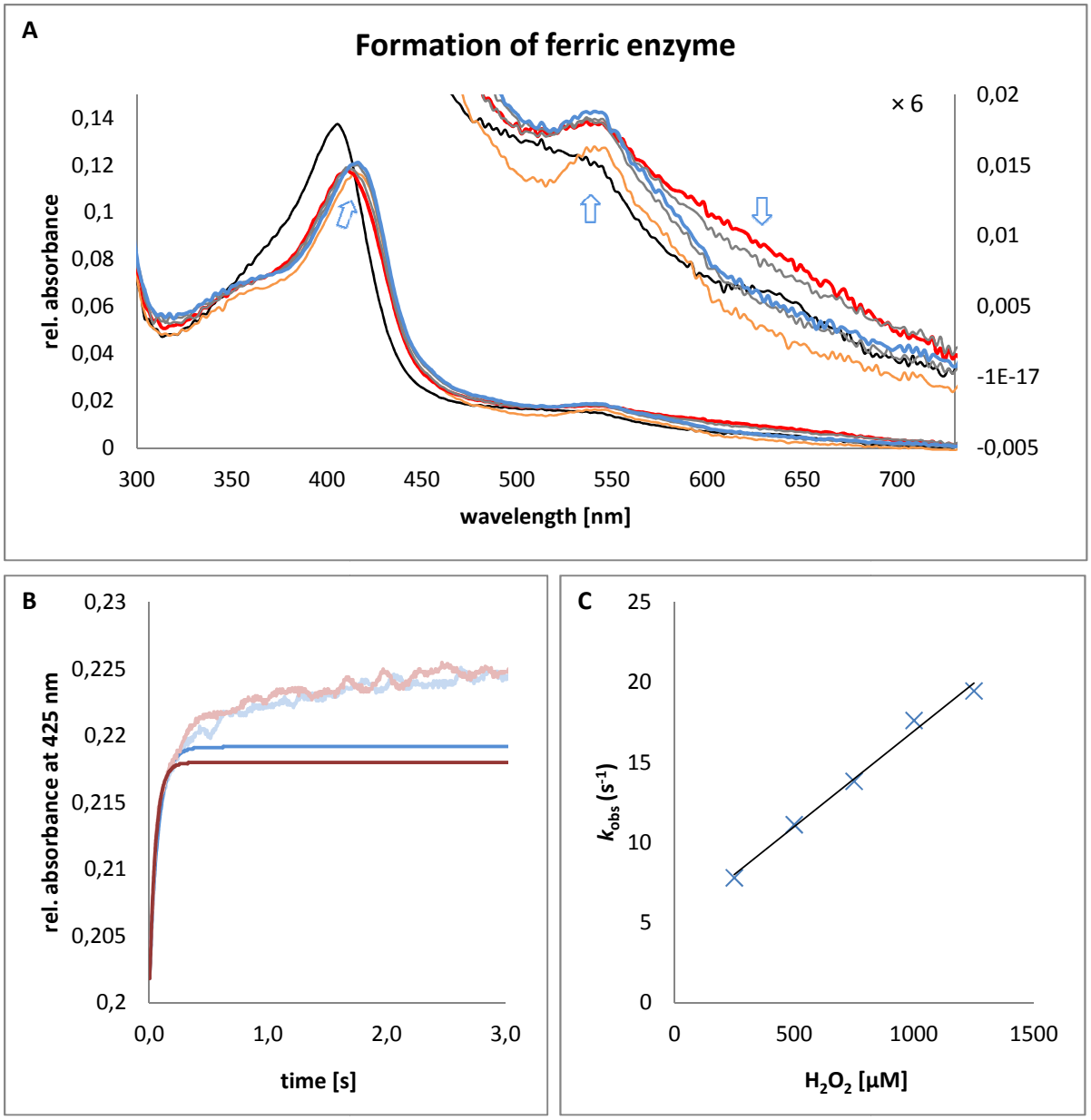

Figure 25: *Reaction of Intermediate I and H_2O_2/CN^-: **A** shows the spectral transition (shown in grey) of Intermediate I (1.2 µM ferric enzyme mixed with 50 µM OCl^-) upon mixing with 1 mM H_2O_2 and 1 mM CN^-. Different states of the enzyme are shown: ferric enzyme (black), Intermediate I (red), Fe(III)-CN^--complex (from pre-formed Intermediate I, blue) and Fe(III)-CN^--complex (ferric enzyme mixed with cyanide, orange). Time traces for two measurements (750 and 1250 µM H_2O_2-concentration, blue and red, respectively) including the single exponential fits can be seen in **B** and **C** shows the determination of k_5 for the formation of ferric enzyme with H_2O_2 (observed rate constants k_{obs} plotted against H_2O_2-concentration).*

Figure 25**A** shows the spectral transition (shown in grey) of Intermediate I (delay time: 100 ms, red spectrum) to the Fe(III)-CN^--complex (blue spectrum). The black spectrum (with a peak maximum at 407 nm) indicates the ferric enzyme and the orange spectrum (with a peak maximum at 417 nm) shows the ferric enzyme-CN^--complex. Isosbestic points of the spectral transition of Intermediate I to the Fe(III)-cyanide-complex can be found at 370 nm and 510 nm.

The reaction of Intermediate I with H_2O_2/CN^- is described by a small increase and a shift in absorbance from 407 to 417 nm. At about 540 and 640 nm a decrease in relative absorbance can be observed while reaction proceeds. The resulting spectrum of this reaction is very similar to the spectrum of the cyanide-complex formed with ferric enzyme and cyanide with appearance of a distinct peak at 540 nm and disappearance of the absorbance at 640 nm, which indicates that the high-spin form was transferred into the low-spin form by binding of cyanide.

Final concentrations used for this test are 1.2 µM MagKatG1, 50 µM OCl^-, 1 mM CN^-, 1 mM H_2O_2, 100 mM phosphate buffer pH 7.0, delay time for Compound I: 100 ms.

Figure 25**B** shows two time traces at 425 – one for the measurement with 750 µM H_2O_2 (light blue) and the other with 1250 µM H_2O_2 (light red) and the corresponding single exponential fits for the initial reaction (marked in dark blue and dark red, respectively). An increase of hydrogen peroxide led to faster reactions and higher k_{obs} were obtained.

The determination of k_5 for the formation of ferric enzyme with H_2O_2 can be seen in Figure 25**C** and was performed in a concentration range from 250 to 1250 µM H_2O_2. Plotting of k_{obs} versus H_2O_2-concentration leads to a linear correlation with a slope of k_5. k_5 for the formation of ferric enzyme with H_2O_2 is $1.2 \times 10^4\ M^{-1}\ s^{-1}$.

6.4.5. Reaction of Intermediate II (formed with OCl^-) and H_2O_2/CN^-

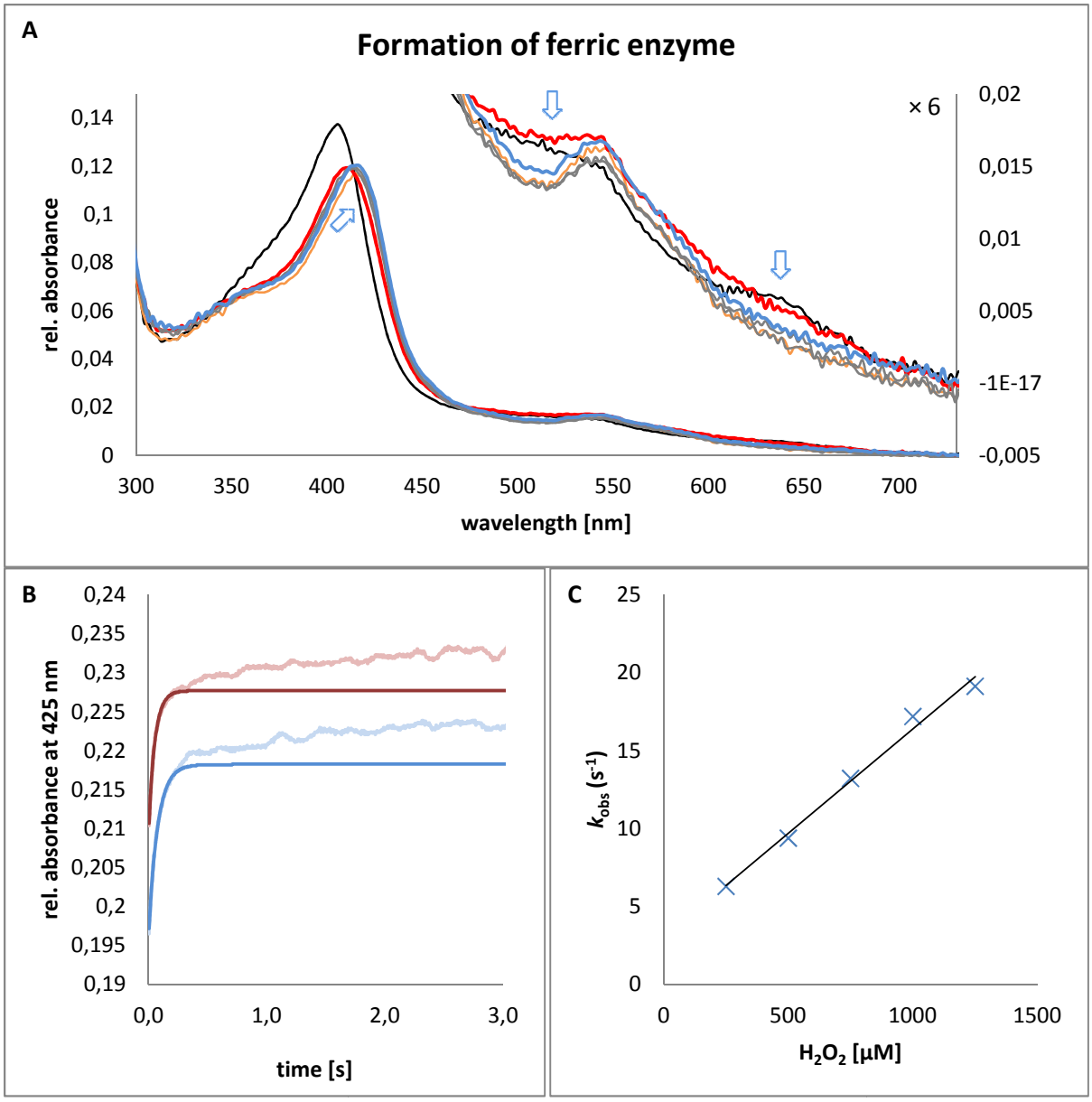

Figure 26: *Reaction of Intermediate II and H_2O_2/CN^-: **A** shows the spectral transition (shown in grey) of Intermediate II (1.2 µM ferric enzyme mixed with 50 µM OCl^-) upon mixing with 1 mM H_2O_2 and 1 mM CN^-. Different states of the enzyme are shown: ferric enzyme (black), Intermediate II (red), Fe(III)-CN^--complex (from pre-formed Intermediate II, blue) and Fe(III)-CN^--complex (ferric enzyme mixed with cyanide, orange). Time traces for two measurements (750 and 1250 µM H_2O_2-concentration, blue and red, respectively) including the single exponential fits can be seen in **B** and **C** shows the determination of k_5 for the formation of ferric enzyme with H_2O_2 (observed rate constants k_{obs} plotted against H_2O_2-concentration).*

Figure 26**A** shows the spectral transition (shown in grey) of Intermediate II (delay time: 1000 ms, red spectrum) to the Fe(III)-CN^--complex (blue spectrum). The black spectrum (with a absorbance maximum at 407 nm) indicates the ferric enzyme and the orange spectrum (with a peak maximum at 417 nm) shows the ferric enzyme-CN^--complex when 1.2 µM ferric enzyme and 1 mM CN^- were mixed. Isosbestic points of the spectral transition of Intermediate II to the Fe(III)-cyanide-complex can be found at 360 nm and 470 nm.

The reaction of Intermediate II with H_2O_2/CN^- is described by a little increase in relative absorption and a shift from 408 to 417 nm. At about 640 nm a decrease in relative absorbance can be observed while reaction proceeds and the decrease at 510 nm lead to a distinct peak at 540 nm. The resulting spectrum of this reaction is very similar to the spectrum of the cyanide complex only formed with ferric enzyme as at 540 nm a peak appeared. The peak at 640 nm disappeared which indicates that the high-spin form was transferred into the low-spin form by binding of cyanide.
Final concentrations used for this test run: 1.2 µM MagKatG1, 50 µM OCl^-, 1 mM CN^-, 1 mM H_2O_2, 100 mM phosphate buffer pH 7.0, delay time for Compound I: 100 ms.

Figure 26**B** shows two time traces at 425 nm – one for the measurement with 750 µM H_2O_2 (light blue) and the other with 1250 µM H_2O_2 (light red) and the corresponding single exponential fits for the initial reaction (marked in dark blue and dark red, respectively). An increase of hydrogen peroxide led to faster reactions and higher k_{obs} were obtained.

The determination of k_5 for the formation of ferric enzyme with H_2O_2 can be seen in Figure 26**C.** The reaction was performed in a concentration range from 250 to 1250 µM H_2O_2. Plotting of k_{obs} against H_2O_2-concentration leads to a linear line with a slope of k_5. k_5 for the formation of ferric enzyme with H_2O_2 is $1.3 \times 10^4\ M^{-1}\ s^{-1}$.

6.4.6. pH dependence

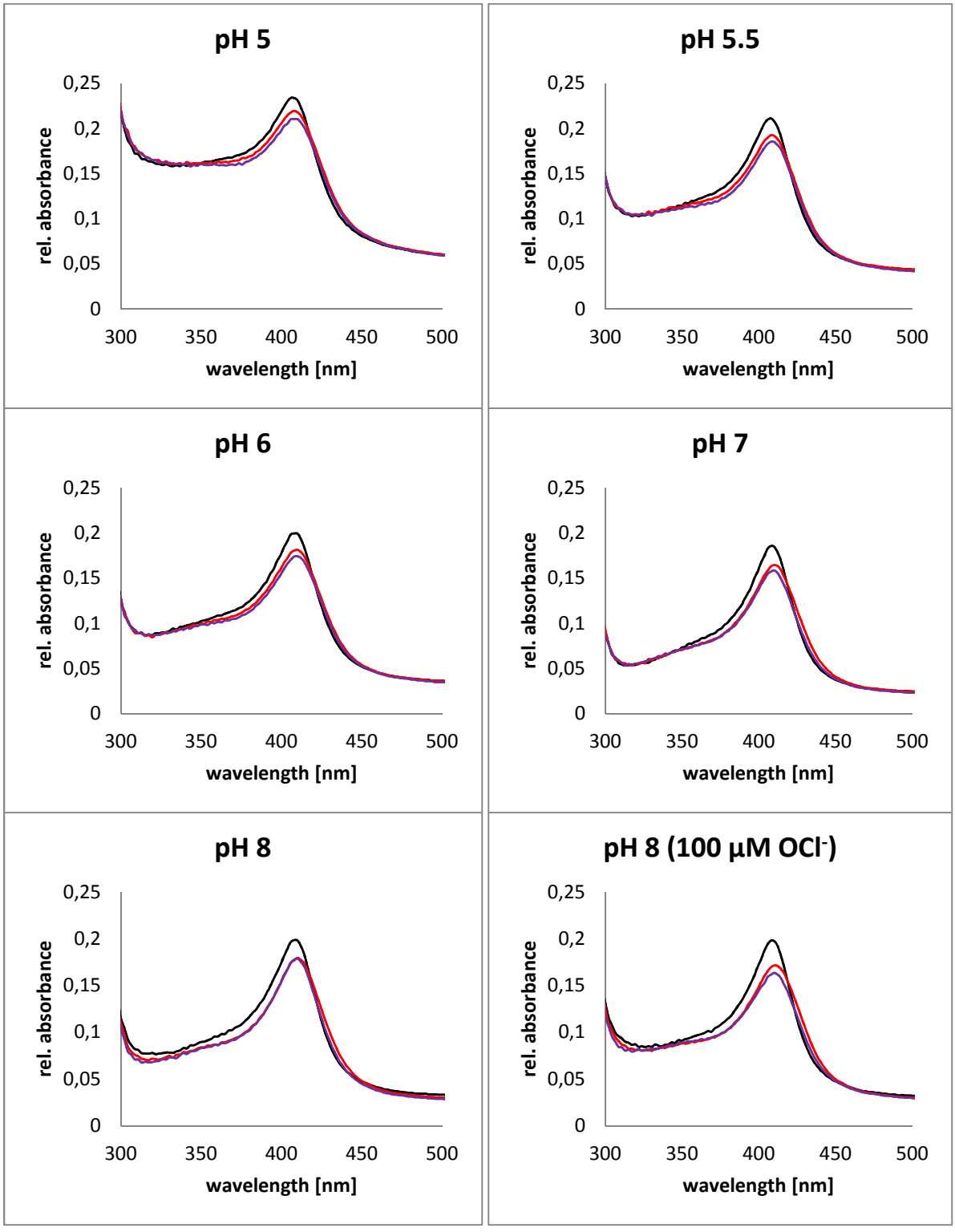

Figure 27: *Reaction of ferric 2 µM MagKatG1 with 50 µM OCl⁻ (pH 5 to 8) and in one case with 100 µM OCl⁻ (pH 8). The black spectrum represents ferric MagKatG1, the red and purple spectra represent Intermediate I and II, respectively.*

These experiments (Figure 27) should show if there is a pH dependence on the transition from Intermediate I to Intermediate II. Both intermediates were observed at pH-values 5, 5.5, 6 and 7 with 50 µM OCl^-. At pH 8, it was not possible to discriminate between these two intermediates so 100 µM OCl^- were used to get a clear distinction. At pH 5 the Q- and CT1-bands are rather low. The higher the pH the more distinct became the peaks at higher wavelengths. Additionally, relative absorbance (within the wavelength range of 300 to 410 nm) was higher at pH 5 and the peaks were not well-defined but are getting clearer at higher pH.

pH	OCl^--conc. [µM]	fit	range [s]	rate [s^{-1}]
5.0	50	single exp.	0.1 - 1.2	3.4
5.5	50	single exp.	0.07 - 1.2	7.0
6.0	50	single exp.	0.07 - 1.2	5.7
7.0	50	single exp.	0.1 - 1.2	6.3
8.0	50	double exp.	0.00128 - 1.2	19.4
8.0	100	single exp.	0.1 - 1.2	1.0

Table 1: *Rates from Intermediate I to Intermediate II at 408 nm with varying pH.*

Table 1 shows the rates varying from 1.0 to 7.0 s^{-1} (single exponential fit). No pH dependence can be observed as the rates are within a small range. The higher value of 19.4 s^{-1} is due to double exponential fit of one run (conditions: pH 8.0, 50 µM OCl^-) as Intermediate I and II could not be discriminated clearly.

7. Summary

Catalase-peroxidases are unique in having both peroxidase and catalase activity. KatGs belong to the Class I of the peroxidase-catalase superfamily and possess two domains per subunit (N-terminal heme-containing domain and C-terminal domain without a cofactor). Phylogenetic analyses of 204 full-length KatG sequences (archaea, bacteria and lower eukaryotes) revealed a horizontal gene transfer event between Bacteroidetes and an ancestor of the sac fungi that led to fungal KatGs. Further steps in evolution led to two distinct groups of catalase-peroxidases: intracellular and extracellular KatGs (KatG1 and KatG2, respectively). The genome of the rice blast fungus *Magnaporthe grisea* has both genes *katg1* and *katg2*. MagKatG2 is shown to be overexpressed at high hydrogen peroxide levels whereas MagKatG1 is expressed constitutively.
Eukaryotic catalase-peroxidases have hardly been investigated. Hence, crystal structures are mainly available for bacterial KatGs and reaction mechanism is proposed for *Synchecocystis* catalase-peroxidase. The main purpose of this work was the determination of the reaction mechanism of eukaryotic KatGs (*M. grisea*) and comparison to bacterial KatGs (*Synechocystis*).

Expression of the recombinant MagKatG1 was done in *E. coli* and purification of the enzyme was achieved by performing two chromatography steps: metal chelate affinity chromatography and hydroxyapatite chromatography. These two steps led to a separation from other proteins and a separation between high-spin and low-spin enzyme. The quality of the purification and molar mass was determined by electrophoresis (SDS-PAGE). Resulting molar mass (of one monomer) of 82.4 kDa correlates with its theoretical molar mass (with one heme *b* and a His_6-tag) of 83.2 kDa.

Spectral characterization was done by using a UV-vis spectrophotometer. The spectrum, which is very similar to the SynKatG spectrum, shows peaks with absorbance maxima at 407 nm (Soret band), 510 and 540 nm (Q-band) and at 635 nm (CT1-band). These peaks indicate the ferric enzyme in high-spin state compared to the low-spin state that is achieved by mixing with cyanide (disappearance of CT1-peak).

Steady-state and pre-steady-state kinetics were determined by using a UV-vis spectrophotometer and a UV-vis stopped-flow apparatus, respectively. The pre-steady-state kinetics represents the main part of this work. Table 2 shows all result of the steady-state an pre-steady-state experiments and compares it with the results of KatG of *Synechocystis*.

MagKatG1 shows a catalase activity of 27 Units/mg and a peroxidase activity of 0.013 Units/mg, which is higher than catalase (10 Units/mg) but lower than peroxidase (0.04 Units/mg) activity of SynKatG. A direct comparison is not possible due to different techniques (SynKatG catalase activity was tested using a Clark electrode) or substrates (SynKatG peroxidase activity was tested using *o*-dianisidine) used for determination of the activities.

Pre-steady-state measurements were performed using the stopped-flow technique as kinetic parameters and spectral changes/intermediates were investigated. Ferric MagKatG1 and peroxyacetic acid formed an intermediate, which could be identified as Compound I showing a hypochromicity with a peak maximum at 410 nm and an increase in relative absorbance with peak maxima at 535 and 640 nm. k_1 for the formation of Compound I with PAA is 1.2×10^4 M^{-1} s^{-1} and is similar to KatG from *Synechocystis*.

During the reaction of ferric MagKatG1 with hypochlorite two intermediates are formed, where the first intermediate (Intermediate I) is most probably equal to Compound I and the second intermediate (Intermediate II) could correspond to Compound I* (radical migration from porphyrin to an amino acid). Rate constant k_1 for the transition of ferric enzyme with hypochlorite could be determined to be 2×10^6 M^{-1} s^{-1}. The transition from Intermediate I to Intermediate II is neither dependent on the concentration of the substrate nor on the pH (was tested within the range from 5.0 to 7.0 and 50 µM OCl^-). At pH 8.0 a concentration of 100 µM OCl^- was used to get a clear discrimination of Intermediate I and Intermediate II.

The reaction of Compound I, Intermediate I and Intermediate II, respectively, with hydrogen peroxide to the ferric enzyme was performed with a mixture of H_2O_2/CN^-. All three rate constants (k_5) are similar (1.2×10^4 M^{-1} s^{-1} – 1.3×10^4 M^{-1} s^{-1}) and comparable to *Synechocystis* catalase-peroxidase (formation of ferric enzyme from Compound I preformed with PAA shows a rate constant of $1.2 \times 10^4 M^{-1} s^{-1}$).

	MagKatG1	SynKatG
Steady-state		
Catalase activity *	27 Units/mg	10 Units/mg
Peroxidase activity **	0.013 Units/mg	- - -
Pre-steady-state		
Formation of Compound I		
with PAA	1.2×10^4 M^{-1} s^{-1}	1.3×10^4 M^{-1} s^{-1}
with OCl^-	2.0×10^6 M^{-1} s^{-1}	- - -
Formation of ferric enzyme with hydrogen peroxide/cyanide		
preformed with PAA	1.2×10^4 M^{-1} s^{-1}	1.2×10^4 M^{-1} s^{-1}
Intermediate I preformed with OCl^-	1.2×10^4 M^{-1} s^{-1}	- - -
Intermediate II preformed with OCl^-	1.3×10^4 M^{-1} s^{-1}	- - -

Table 2: *Overview of steady-state and pre-steady-state kinetic parameters. *Catalase activity for Synechocystis KatG was determined using a Clark-type electrode. **Different substrates were used for determination of peroxidase activity.*

Pre-steady state rate constants of MagKatG1 are similar to SynKatG concluding that the reaction mechanism is similar and follows the sequence:

Ferric enzyme → Compound I → Compound I* → Compound III* → Ferric enzyme

Spectral changes from ferric enzyme to Compound I and back could be shown. Other intermediates shown in the reaction scheme (Compound I* or Compound III*) could not be clearly identified. Further experiments and investigations need to be done to eluciate the full reaction mechanisms of MagKatG1 and eukaryotic KatGs.

8. Abbreviations

aa	Amino acid
AH_2	One-electron donor
APx	Ascorbate peroxidase
Arg	Arginine
Asn	Asparagine
Asp	Aspartic Acid
BCIP	5-bromo-4-chloro-indolyl-phosphate
CcP	Cytochrome *c* peroxidase
CFEM	Conserved fungal-specific extracellular membrane
GMO	Genetically modified organism
GPCR	G-protein-coupled receptor
HA	Hydroxyapatite
$HA^{\bullet}$	Corresponding radical of a one-electron donor
H_2O_2	Hydrogen peroxide
HGT	Horizontal gene transfer
His	Histidine
HS	High spin
IPTG	Isopropyl-β-D-thiogalactoside
KatG	Catalase-peroxidase
kDa	kilo Dalton
k_{obs}	observed rate constant
LS	Low spin
MAPK	Mitogen-activated protein kinase
MCAC	Metal chelate affinity chromatography
Met	Methionine
NBT	Nitro blue tetrazolium
PAA	Peroxyacetic acid
PBS	Phosphate buffered saline
PMFS	Phenylmethylsulfonyl fluoride
ROS	Reactive oxygen species
SDS-PAGE	Sodium dodecyl sulfate-polyacrylamide gel electrophoresis
Trp	Tryptophan
Tyr	Tyrosine

9. References

R. A. Dean et al., 2005, The genome sequence of the rice blast fungus *Magnaporthe grisea*, Nature, Volume 434, 980 – 986

L. J. Donald, O. V. Krokhin, H. W. Duckworth, B. Wiseman, T. Deemagarn, R. Singh, J. Switala, X. Carpena, I. Fita, P. C. Loewen, 2003, Characterization of the catalase-peroxidase KatG from *Burkholderia pseudomallei* by mass spectrometry, J. Biol. Chem. 278 (37), 35687 – 35692

C. Jakopitsch, G. Regelsberger, P. G. Furtmüller, F. Rüker, G. A. Peschek, C. Obinger, 2001, Catalase-Peroxidase from *Synechocystis* is capable of chlorination and bromination reactions, Biochem. Biophys. Res. Commun. 287 (3), 682 – 687

C. Jakopitsch, M. Auer, G. Regelsberger, W. Jantschko, P. G. Furtmüller, F. Rüker, C. Obinger, 2003a, The catalytic role of the distal site asparagines-histidine couple in catalase-peroxidases, Eur. J. Biochem. 270, 1006-1013

C. Jakopitsch, M. Auer, G. Regelsberger, W. Jantschko, P. G. Furtmüller, F. Rüker, C. Obinger, 2003b, Distal Site Aspartate Is Essential in the Catalase Activity of Catalase-Peroxidases, Biochemistry 43, 5292-5300

C. Jakopitsch, D. Kolarich, G. Petutschnig, P. G. Furtmüller, C. Obinger, 2003c, Distal side tryptophan, tyrosine and methionine in catalase-peroxidases are covalently linked in solution, FEBS Lett. 552, 135-140

C. Jakopitsch, J. Vlasits, B. Wiseman, P. C. Loewen, C. Obinger, 2007, Redox intermediates in the catalase cycle of catalase-peroxidase from *Synechocystis* PCC 6803, *Burkholderia pseudomallei* and *Mycobacterium tuberculosis,* Biochemistry 46 (5), 1183 – 1193

J. Vlasits C, Jakopitsch M, Schwanninger P, Holubar C.Obinger 2007, Hydrogen peroxide oxidation by catalase-peroxidase follows a non-scrambling mechanism. FEBS Lett. 581 (2), 320-324

J. Vlasits, C. Jakopitsch, M. Bernroitner, M. Zamocky, P. G. Furtmüller, C. Obinger, 2010a, Mechanisms of catalase activity of heme peroxidases, Arch. Biochem. Biophys. 500, 74 – 81

J. Vlasits, P. G. Furtmüller, C. Jakopitsch, M. Zamocky, C. Obinger, 2010b, Probing hydrogen peroxide oxidation kinetics of wild-type *Synechocystis* catalase-peroxidase (KatG) and selected variants, Biochem. Biophys. Acta 1804, 799 – 805

M. Zamocky, P. G. Furtmüller, C. Obinger, 2009a, Two distinct groups of fungal catalase/peroxidases, Biochem. Soc. Trans. 37 (4), 772 – 777

M. Zamocky, P. G. Furtmüller, M. Bellei, G. Battistuzzi, J. Stadlmann, J. Vlasits, C. Obinger, 2009b, Intracellular catalase/peroxidase from the phytopathogenic rice blast fungus *Magnaporthe grisea*: expression analysis and biochemical characterization of the recombinant protein, Biochem. J. 418, 443 – 451

M. Zamocky, C. Obinger, 2010, Chapter 2 – Molecular Phylogeny of Heme Peroxidases, Biocatalysis Based on Heme Peroxidases, Springer-Verlag Berlin Heidelberg

M. Zamocky, B. Gasselhuber, P. G. Furtmüller, C. Obinger, 2012a, Molecular evolution of hydrogen peroxide degrading enzymes, Arch. Biochem. Biophys. 525, 131 – 144

M. Zamocky, E. Droghetti, M. Bellei, B. Gasselhuber, M. Pabst, P. G. Furtmüller, G. Battistuzzi, G. Smulevich, C. Obinger, 2012b, Eukaryotic extracellular catalase-peroxidase from *Magnaporthe grisea* – Biophysical/chemical characterization of the first representative from a novel phytopathogenic KatG group, Biochimie 94, 673 – 683

M. Zamocky, Q. Garcia-Fernandez, B. Gasselhuber, C. Jakopitsch, P. G. Furtmüller, P. C. Loewen, I. Fita, C. Obinger, X. Carpena, 2012c, High conformational stability of secreted eukaryotic catalase-peroxidases – J. Biol. Chem. 287 (38), 32254 - 32262